8. Geochemical Evidence for the Sedimentary and Diagenetic Development of the Mesozoic–Early Cenozoic Newfoundland Rifted Margin, Northwest Atlantic (Ocean Drilling Program Leg 210, Site 1276)[1]

Alastair H.F. Robertson[2]

ABSTRACT

Inorganic chemical composition and downhole variation of major and trace elements yields useful insights into the sediment provenance and paleoceanography of deep-sea sediments of deepwater continental margins. Here, fine-grained sediments were chemically analyzed at ~10-m intervals from the Eocene to Albian section at Site 1276. These sediments represent a time when background hemipelagic sedimentation was continuously beneath, or near, the calcite compensation depth (CCD). Additional samples were analyzed from the upper Paleocene–middle Eocene time interval to determine whether a volcaniclastic component is present, as suggested by petrographic studies of the coarser size fraction. Sediments recovered near the bottom of the hole show the effects of contact metamorphism adjacent to a sill of alkaline basalt. The overlying thick (~700 m) Albian succession (lithologic Unit 5) is indicative of a dominantly terrigenous source. Redox-sensitive trace elements (e.g., Cu, Ni, V, and Cr) are concentrated in organic-rich layers (black shales) that can be partially correlated with oceanic anoxic Events 1a–1d and 2. Beginning around the Cenomanian/Turonian boundary, a profound change took place to more oxidizing, slowly depositing sediments throughout the North Atlantic, characterized by relative enrichment in Fe, Mn, and related trace metals (e.g., Cu, Ni, and

Cr). Similar background conditions persisted until the Eocene when local conditions at Site 1276 became more reducing, as indicated by more subdued colors and lower MnO contents. Moderate upwelling along the Newfoundland continental margin during the Eocene is suggested by the presence of relatively high values of silica coupled with opaline silica. Phosphate and associated trace elements (e.g., Ce and Y) are locally enriched, suggesting relatively high primary productivity. However, productivity was lower than on the conjugate Iberia margin at Deep Sea Drilling Project Site 398. Fine-grained terrigenous sediments at Site 1276 probably were mainly derived from the Grand Banks (e.g., Avalon uplift) and finally accumulated in deep water below the CCD mainly as mud turbidites and hemipelagites.

INTRODUCTION

The aim of this paper is to use inorganic geochemical analysis of fine-grained sediments to shed light on the depositional and diagenetic processes related to the development of the Mesozoic–early Cenozoic rifted margin of the northwest Atlantic Ocean off Newfoundland (Canada), as sampled during Leg 210 (Tucholke, Sibuet, Klaus, et al., 2004). Site 1276 is located at the base of the continental rise east of the Grand Banks/Flemish Cap (Figs. F1, F2). Chemical data presented here complement the information from core descriptions, smear slide analysis, X-ray diffraction (XRD), and preliminary chemical analysis, as obtained at sea (Shipboard Scientific Party, 2004). Analysis of chemical changes in fine-grained sediments through time is useful to identify changes in sediment provenance, paleoceanography, and diagenesis. Despite this, published geochemical analyses of deep-sea sediments that cover a long time-range, as presented here, remain remarkably rare.

Fine-grained sediments that were studied represent a combination of background hemipelagic sediments and the fine-grained upper intervals of turbidites, which in many instances cannot be easily distinguished from one another in the cores (Shipboard Scientific Party, 2004). These sediments experienced extensive mixing during sediment transport, prior to final deposition, and are therefore likely to record the composition of a range of source rocks exposed over a wide area in the region of sediment supply. Sand-sized sediment was studied petrographically in a related study (Marsaglia et al., this volume).

GEOLOGICAL SETTING

The local setting of Site 1276 on the Newfoundland rifted margin is shown in Figure F2. Note its location between basement highs to the northwest that are known to be rifted continental crust and crust to the southeast, which is located within the ocean–continent transition zone. The regional U reflection (Fig. F2) that was penetrated at Site 1276 was initially thought simply to record a break-up unconformity (Tucholke et al., l989). However, results at Site 1276 suggest that it may also be related to the regional intrusion of alkaline basalt sills following final continental break-up (Shillington et al., 2006). Seaward of Site 1276, exhumed mantle serpentinite and overlying basaltic flows were recovered within the ocean–continent transition zone at Site 1277 (Shipboard Scientific Party, 2004; Robertson, this volume).

F1. Location of Site 1276, p. 22.
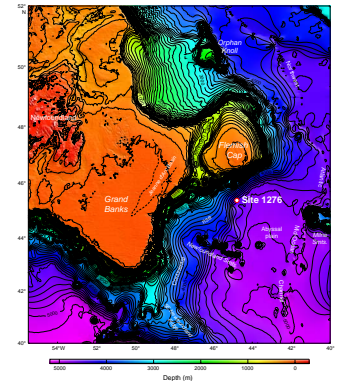
F2. Seismic profiles, p. 23.
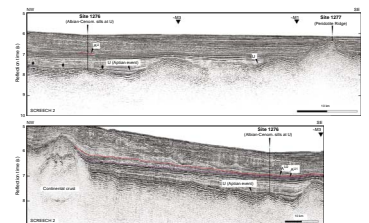
At Site 1276, a single deep hole was drilled at the lower edge of the continental rise and was cored from 800 to 1739 meters below seafloor (mbsf) (Fig. F2). Cored sediments begin with deep-sea sediments of earliest Oligocene age and end with deep-sea sediments of earliest Albian age (Fig. F3). A latest Aptian age was suspected for the oldest sediments, but this has not been confirmed. An excellent, relatively complete sedimentary record (~85%) was obtained for the cored interval. The oldest sediments significantly postdate the crust, which is estimated at ~130 Ma (i.e., end-Hauterivian). Coring terminated within the lower of two sills of alkaline basalt, which intruded at ~105 and ~98 Ma (Hart and Blusztajn, 2006). Intrusion of these sills has influenced the diagenesis of the directly adjacent sediments recovered from Site 1276 (Shipboard Scientific Party, 2004; Pletsch and Cramer, 2006).

In general, sediment recovery documents the evolution of a rifted passive continental margin following regional continental break-up. Deposition first took place on a thermally immature, rapidly subsiding, topographically varied rifted margin on which very rapid sediment accumulation took place at rates up to 105 mm/yr. During this time only a narrow (~100 km) deep-ocean basin separated Site 1276 from the conjugate Iberia margin. This was followed by a more thermally mature phase during which subsidence slowed and sedimentation rates decreased greatly to <7.4 mm/yr. During this time Site 1276 bordered an increasingly wide oceanic basin.

A summary of sediments recovered and their ages is given in Figure F3. The grain-size plot in this figure emphasizes the occurrence of relatively coarse grained sediments that were mainly deposited by turbidity currents (Shipboard Scientific Party, 2004). However, the present paper focuses on the chemical composition and interpretation of the fine-grained sediments, which volumetrically predominate.

METHODS AND MATERIALS

Analytical Data

Inorganic chemical analysis of 102 samples of fine-grained sediments was carried out by X-ray fluorescence (XRF) at the University of Edinburgh (United Kingdom), School of GeoSciences, using the method described below.

Representative fine-grained sediments were selected for analysis at an interval of one per core (i.e., one sample per ~10 m). Exceptions were made where, occasionally, fine-grained sediments were not present within a particular core or where samples inadvertently were not taken. Despite being of considerable interest, the Cretaceous/Cenozoic boundary interval did not include fine-grained sediments and was not sampled during this work. Also, occasional black-shale intervals (Fig. F3) that were thought to represent rare well defined oceanic anoxic events (OAEs) were not sampled because they were reserved for more specialized analysis (see Arnaboldi and Meyers, this volume). However, some of the large number of organic-rich sediment layers within the Albian–Cenomanian interval were sampled and geochemically analyzed during this work. Additional samples of fine-grained sediments were analyzed from the upper Paleocene–middle Eocene time interval (Unit 2) to determine whether a volcaniclastic component is present. Volcaniclastic material was observed in sand-sized turbidites from this interval (Ship-

F3. Summary of core recovery, p. 24.
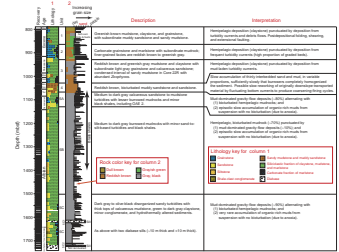
board Scientific Party, 2004; Marsaglia et al., this volume), with significant implications for sediment provenance and regional geology.

X-Ray Fluorescence Analysis

The analytical method for major and trace elements was described by Fitton et al. (1998) and is repeated below in slightly modified form. Major element concentrations were determined after fusion with a lithium borate flux containing La_2O as a heavy absorber using a standard method referred to by Fitton et al. (1998). Rock powder was dried at 100°C for at least 1 hr, and a nominal but precisely weighed 1-g aliquot was ignited at 1100°C to determine loss on ignition (LOI). The residue was then mixed with Johnson Matthey Spectroflux 105 in a sample to a flux ratio of 1:5, based on the unignited sample mass, and was fused at 1100°C in a muffle furnace in a Pt 5% Au crucible. After the initial fusion, the crucible was reweighed and any flux weight loss was made up with extra flux. After a second fusion over a Meker burner, the molten mixture was swirled several times to ensure homogeneity, cast into a graphite mold, and flattened with an aluminium plunger into a thin disk. The mold and plunger were maintained at a temperature of 230°C on a hotplate.

Trace element concentrations were determined on pressed-powder samples. Eight grams of rock powder were mixed with eight drops of a 2% aqueous solution of polyvinyl alcohol and then formed into a 38 mm diameter disc backed and surrounded by a 0.3-mm aluminium foil "cup" and compressed in a hydraulic press to produce a solid disc.

Fused and pressed samples were analyzed using a Phillips PW 1480 automatic XRF spectrometer with a Rh-anode X-ray tube. Analytical conditions and calibrations were optimized for low concentrations of trace elements. Background positions were placed close to peaks, and long count times were used at both peak and background positions. Where background count rates were measured on either side of the peak, as in most trace element determinations, the count time was divided equally between the two positions. The analytical conditions are specified in table 2 of Fitton et al. (1998).

Corrections for matrix effects on the intensities of major element lines were made using theoretical alpha coefficients calculated online with Phillips software. Coefficients were calculated to allow for the amount of extra flux replacing volatile components in the sample so that analytical totals could be 100%, less the measured LOI. Intensities of longer wavelength trace element lines (La, Nd, Cu, Ni, Co, Cr, V, Ba, and Sc) were corrected for matrix effects using alpha coefficients based on major element concentrations measured at the same time on powder samples. Matrix corrections were applied to intensities of other trace element lines by using the count rate from the Rh Kalpha Compton scatter line as an internal standard. Line-overlap corrections were applied using synthetic standards.

The spectrometer was calibrated with United States Geological Survey and Centre de Recherches Petrographiques et Geochimiques standards, using the standard values referred to by Fitton et al. (1998). These standards were run prior to and after the sample analyses. Additional in-house standards were used to fine-tune calibrations for each analytical run. Independent in-house standards, not used for the spectrometer calibration, were also analyzed during each run. Details of precision and accuracy determined for the above analytical method are given in Fitton et al. (1998).

Inorganic geochemical data obtained during this study are set out as weight-percent oxides for major elements and parts per million for trace elements (Table T1).

Associated Data

Supporting data used here include core descriptions, smear slide and thin section descriptions, clay mineral identifications, and carbonate determinations. This information is reported in the "Lithostratigraphy" section of Shipboard Scientific Party (2004).

Additional inorganic chemical analyses were obtained at sea using the inductively coupled plasma–atomic emission spectrometry (ICP–AES) method (see Tucholke, Sibuet, Klaus, et al., 2004). Analyzed shipboard samples typically include a range of different lithologies and grain sizes, and they were selected for analysis to aid immediate identification and initial interpretation of the sediments. Shipboard and postcruise studies were therefore carried out using different analytical techniques. It is unwise simply to treat all of the analytical data as a single database, and this paper focuses on the new XRF analyses. In general, results given here support and complement the preliminary interpretations of the ICP–AES data given in Shipboard Scientific Party (2004). Some of the dark organic-rich sediments (black shales), including designated OAEs, were also analyzed at sea for major and trace elements by the ICP–AES method. Black shales were also analyzed for total organic carbon (TOC) at sea by the Rock-Eval pyrolysis method (see Tucholke, Sibuet, Klaus, et al., 2004). Additional geochemical data for the black shales were obtained postcruise and are reported by Arnaboldi and Meyers (this volume).

DISCUSSION AND INTERPRETATION OF RESULTS

Inorganic geochemical data are interpreted here in relation to the sedimentary development of Site 1276. The succession is discussed from the base upwards to help identify changes though time. The discussion below is organized into five time intervals, which correspond to the lithological units recognized at sea (Fig. F3). A summary of the inferred depositional setting of the fine-grained sediments deposited during each of these time intervals is given first. Relevant inorganic geochemical data from this study are then integrated, with reference to selected geochemical plots. A brief comparison with coeval sediments recovered elsewhere in the North Atlantic is then made. Finally, sediment provenance and the origin of the black shales are discussed for the site as a whole.

Albian–Turonian (Unit 5)

Sedimentology

The Albian–Turonian interval at Site 1276 (>700 m thick) was divided by the shipboard sedimentologists into three subunits, mainly on the basis of color, degree of bioturbation, and carbonate content, as summarized in Figure F3. This time interval contains several organic-rich layers with >1 wt% organic matter, as determined at sea, which were described as black shales.

Subunit 5C is of Albian age and contains >80 intervals of mudrocks that were determined to be turbidites, mainly based on the sedimentary

structures observed in the cut core faces at sea. This time interval also includes coarser grained sediments that were interpreted as mud-rich turbidites, sand-rich turbidites, and muddy and sandy debris flows. Burrowing is rare or absent. The presence of occasional reddish layers is suggestive of periodically oxidizing bottom conditions, whereas the succession overall is mainly anoxic. Highly altered volcanic ash was locally identified. Pyritized radiolarians were occasionally noted in smear slides from the upper Albian interval. Agglutinated foraminifers are rarely present.

Subunit 5B, of Albian–Cenomanian age, is 90% mudrock, which is generally well burrowed and indicates a change to generally oxidizing bottom conditions during this time. This interval has a greater proportion of background hemipelagic sediment compared to the subunits above and below, as suggested by shipboard smear slide analysis. TOC values determined at sea are generally lower than those in Subunit 5A (Shipboard Scientific Party, 2004). Beginning in the Cenomanian (and extending through the Maestrichtian to Paleogene), the planktonic foraminifer assemblage is indicative of a relatively cool water boreal influence (Shipboard Scientific Party, 2004).

Subunit 5A, of Cenomanian–Turonian age, is largely devoid of bioturbation and includes numerous sand and mud turbidites (~71% of the succession). The coarser grained fraction contains abundant metamorphic rock fragments, mainly quartzite and mica schist. In addition, occasional black layers exhibit relatively high TOC values (reported in Shipboard Scientific Party, 2004). OAE 2 was identified in Sections 210-1276A-31R-3 and 31R-4. Shipboard inorganic chemical analysis was carried out on several samples from the inferred OAE 2 horizon by the ICP–AES method, and these are enriched in Ca, MnO, P_2O_5, Cr, Ni, Fe, and V relative to the interbedded nonorganic-rich mudrocks. Also, Al_2O_3, TiO_2, and other lithogenous constituents are depleted within the black shale layers relative to the less organic rich mudrocks above and below. Palynomorphs are relatively abundant, whereas calcareous microfossils are sparse and usually poorly preserved. Wood and plant fragments are common, indicating an important terrigenous input (Shipboard Scientific Party, 2004). In addition, shipboard Rock-Eval pyrolysis suggested that the organic matter in these black shales is commonly, but not exclusively, terrestrial.

Taking Unit 5 as a whole, shipboard XRD analysis detected quartz, clay minerals, and feldspar (plagioclase and alkaline). Clay minerals are illite-smectite, mixed-layer clays, illite, muscovite, chlorite, and kaolinite group minerals. The favored shipboard interpretation of the clay mineral occurrence is that during the Albian–Turonian (a time of rising sea level [Haq et al., 1987]), particulate land-derived kaolinite and chlorite were largely trapped on the continental shelf, whereas the largely colloidal illite-smectite bypassed the margin to reach the deep basin (McCave, 1972; Chamley, 1979; Robertson and Bliefnick, 1983; Chamley and Debrabant, 1984; Stow et al., 2001).

The lowest part of the Unit 5 succession included two sills of alkaline basalt, of which only the upper sill and its adjacent sediments were completely penetrated. During postcruise studies the age of the upper sill was estimated to be 82.5–105.9 Ma (Karner and Shillington, 2005), based on the porosity vs. depth trend in the sediments. More recently, the sills yielded $^{40}Ar/^{39}Ar$ plateau ages of ~105.3 Ma for the upper sill and ~97.8 Ma for the lower sill (Hart and Blusztajn, 2006). Calcareous mudstones directly above the upper sill contain numerous porphyroblasts of pure stoichiometric calcite in which inclusions of crystalline

albite, sodaite (magnesian chlorite), possible magnesium calcite, and pyrite were identified by shipboard XRD. There is evidence of a change from smectite of inferred detrital origin to illite-smectite mixed layer clays of diagenetic origin ~100 m above the upper sill. This could reflect a diagenetic change related to depth of burial, local thermal effects from the sills beneath, or a change in the composition of source clays, related to climatic change on land (Pollastro, 1993; Pletsch, 1997). Post-cruise studies using vitrinite reflectance of organic matter suggest that, except in close proximity to the sills, the thermal maturity of the sedimentary succession remained outside the oil-generating window; even close to the sills the dominant kerogen did not favour hydrocarbon generation (Pletsch and Cramer, 2006). A study of the thermal alteration of six sporomorphs groups also shows that thermal alteration does not increase until within ~20 m of the igneous sill, a step rise occurs at 4.23 m above the sill, and the strongest alteration is seen in the sample closest to the sill (Pross et al., 2007).

Geochemistry

A relatively large number of samples (63) were analyzed from the long Albian–Turonian interval represented by Unit 5 (Table T1). A cross-plot of Al_2O_3 vs. K_2O (Fig. F4) shows a strong positive correlation, consistent with the presence of a compositionally constant detrital material, probably detrital clay input. A crossplot of Al_2O_3 vs. MgO (Fig. F5) shows scatter that suggests the presence of more than one detrital constituent or a single constituent of variable composition (e.g., different states of chemical alteration or diagenesis). In common with other areas of the North Atlantic, Al_2O_3, K_2O, and MgO are assumed to be mainly detrital in origin (Chamley and Debrabant, 1984). The crossplot of Al_2O_3 vs. Na_2O (Fig. F6) shows a similar scatter. However, the stratigraphically lowest sample analyzed in close proximity to a diabase sill shows a very high value of Na_2O (~3.26 wt%). This is assumed to record the formation of a Na-bearing phase, possibly a clay mineral, feldspar, or zeolite, in response to locally elevated temperature close to the sill (Shipboard Scientific Party, 2004).

Analyzed samples show a general correlation of Al_2O_3 and TiO_2 (Fig. F7). However, some samples are relatively enriched in TiO_2. This suggests that a compositionally different Ti-rich source material may be present (e.g., a volcaniclastic turbidite or tuff of alkaline composition). Very altered fine-grained tuff was locally observed in smear slides near the Subunit 5B/5C boundary, suggesting that a fine-grained but highly altered Ti-rich tuffaceous component may be present. The relative TiO_2 variation may also relate to compositional differences in the source lithologies located on the adjacent continental margin, which could include a Ti-rich component (e.g., rift-related alkaline igneous rocks).

A crossplot of MgO vs. TiO_2 (Fig. F8) confirms the existence of a persistent terrigenous component but with considerable compositional variation. A crossplot of Al_2O_3 vs. Fe_2O_3 (Fig. F9) also suggests a terrigenous association but with considerable scatter and several relatively Fe_2O_3 rich samples, which probably reflect diagenesis (see below).

The Al_2O_3 vs. SiO_2 cross-plot (Fig. F10) reveals two general compositional groupings. First, a "detrital" grouping shows a positive correlation of Al_2O_3 and SiO_2. The second grouping is relatively enriched in SiO_2 and shows a generally negative correlation. This probably reflects

F4. Al_2O_3 vs. K_2O, Unit 5, p. 25.
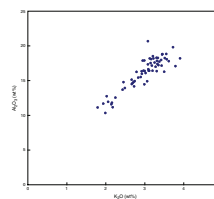
F5. Al_2O_3 vs. MgO, Unit 5, p. 26.
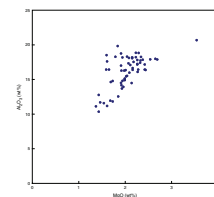
F6. Al_2O_3 vs. Na_2O, Unit 5, p. 27.
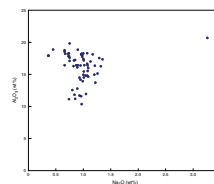
F7. Al_2O_3 vs. TiO_2, Unit 5, p. 28.
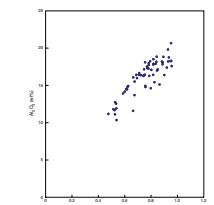
F8. MgO vs. TiO_2, Unit 5, p. 29.
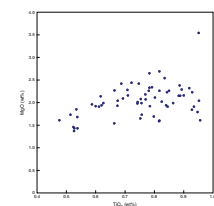
F9. Al_2O_3 vs. Fe_2O_3, Unit 5, p. 30.
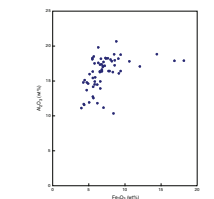
the presence of biogenic silica (i.e., a siliceous component independent of quartz associated with detrital aluminosilicates).

A plot of Fe_2O_3 vs. MnO (Fig. F11) suggests that the two metal oxides occur independently of each other. The local enrichment in MnO could suggest the presence of an insoluble diagenetic phase (e.g., manganese carbonate), although this was not detected by shipboard XRD. A number of samples are relatively enriched in Fe_2O_3 (up to 18%) and are also relatively rich in CaO, which is otherwise very low in these sediments that accumulated below the calcite compensation depth (CCD). The combined relative enrichment of Fe_2O_3 and CaO is attributed to the diagenetic formation of siderite, as revealed by shipboard XRD. MgO is not, however, similarly enriched in the ferruginous samples, suggesting that dolomite is not significantly abundant as a diagenetic phase, in agreement with shipboard XRD.

Regional Comparisons

A detailed comparison can be made with the equivalent Albian time interval at Deep Sea Drilling Project (DSDP) Site 398 on the conjugate Iberia margin, which is <100 km east of Site 1276 on a restored palaeogeography (Tucholke, Sibuet, Klaus, et al., 2004). Similar sedimentation persisted at Site 398 from the upper Barremian through the upper Aptian, a longer time interval than at Site 1276 where no pre-Albian succession has been drilled.

The oldest sediments recovered at Site 398, of Barremian–Albian age, are similar to those of Subunit 5C at Site 1276 but are largely older and are more obviously turbiditic. A relatively shallow water prodelta setting or a deeper water submarine fan setting was suggested for these sediments at Site 398 (Arthur, 1979). By contrast, their younger counterparts at Site 1276 accumulated in a deeper water bathyal setting below the CCD (Shipboard Scientific Party, 2004). At Site 398 the Albian sediments, as at Site 1276, are relatively organic rich and contain low Ca and abundant plant debris. The lower to mid-Albian intervals at both of these sites accumulated at more or less the same rates (i.e., 20–100 mm/yr). A probable equivalent of OAE 2, as recognized at Site 1276, was identified within the mid-Cenomanian to mid-Albian interval at Site 398 (Sibuet, Ryan, et al., 1979; de Graciansky and Chenet 1979).

In addition, time equivalents of Unit 5 were cored at several DSDP sites in the central North Atlantic, where lithologically similar sediments range from Barremian to Cenomanian in age. This interval is mainly carbonates and clays of greenish gray and black shales, together with some calcareous sediments and laminated marls (Jansa et al., 1979; Meyers, 1987). The black shales can be generally correlated with the OAEs identified at Site 1276. The DSDP sites are located farther off-margin and therefore contain relatively little sand compared to Site 1276. However, many of the hemipelagic sediments in these more distal settings are interpreted to have accumulated as low-density turbidites (McCave 1979; Robertson and Bliefnick, 1983), similar to the mudrocks recovered at Site 1276.

F10. Al_2O_3 vs. SiO_2, Unit 5, p. 31.
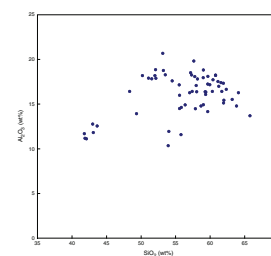
F11. Fe_2O_3 vs. MnO, Unit 5, p. 32.
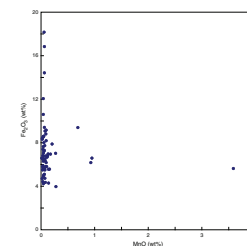
Turonian–Uppermost Santonian (Unit 4)

Sedimentology

At Site 1276, the Turonian to uppermost Santonian interval is characterized by reddish brown strongly bioturbated muddy sandstones and siltstones. These sediments are mainly siliciclastic, with only very minor intercalated mudrocks. The sparse mudrocks contain quartz, calcite, plagioclase, alkali feldspar, smectite, minor illite, rare kaolinite, chlorite, goethite, manganite, and also manganese hydroxide as thin layers (Shipboard Scientific Party, 2004).

The Turonian- to uppermost Santonian–aged sediments are stratigraphically condensed and accumulated at a slow rate (~1.9–4.0 mm/yr). Where present, these mudrocks accumulated in a strongly oxidizing setting, hence their reddish color. Clay mineralogy indicates that the terrigenous material was derived from a landmass that experienced weathering in a warm humid climate (Chamley, 1989). The contrasting silty and sandy nature of much of Unit 4 is attributed to the activity of relatively strong bottom currents. This was possibly associated with the establishment of a deep-marine connection with the South Atlantic around the Cenomanian/Turonian boundary (Tucholke and Vogt, 1979). An alternative is that the oxidizing environment relates to the separation of the Rockall Plateau from northwest Europe (Sibuet, Ryan, et al., 1979). However, the relatively small geographical scale of this event is unlikely to have triggered such a major oceanographic change affecting the entire North Atlantic.

Geochemistry

Interelement relationships are combined for Units 3 and 4 because the number of samples analyzed is relatively small. The crossplots of Al_2O_3 vs. TiO_2 (Fig. F12) and Al_2O_3 vs. K2O (Fig. F13) confirm the presence of a dominantly terrigenous component, similar to Unit 5. By contrast, Al_2O_3 vs. SiO_2 (Fig. F14) shows a clear inverse correlation, which is attributable to the presence of biogenic silica. Locally high concentrations of MnO (up to 2.58 wt% MnO) are associated with relatively high Cu, Zn, and Ni (Table T1). A manganese oxide mineral phase was detected by shipboard XRD. The metal enrichment is consistent with strong oxidization at the seafloor.

Regional Comparisons

At Site 398, the upper Turonian–Campanian interval is dominated by reddish brown nonfossiliferous claystones (Sibuet, Ryan, et al., 1979). However, these sediments do not show an enrichment of trace metals comparable to Site 1276 (Chamley et al., 1979), although the data set is less complete for Site 398. Similar sediments also occur elsewhere on the Iberia margin at Ocean Drilling Program (ODP) Sites 899, 898, and 1070, but their age is not well constrained (Sawyer, Whitmarsh, Klaus, et al., 1994; Beslier, Whitmarsh, Wallace, and Girardeau, 2001). Also, these sediments have not been studied geochemically. Comparable sediments from the central Atlantic are mentioned below.

F12. Al_2O_3 vs. TiO_2, Units 3 and 4, p. 33.
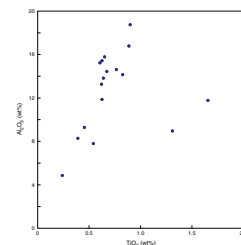
F13. Al_2O_3 vs. K_2O, Units 3 and 4, p. 34.
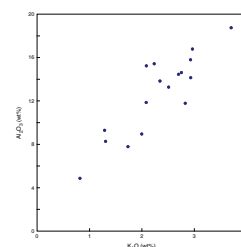
F14. Al_2O_3 vs. SiO_2, Units 3 and 4, p. 35.
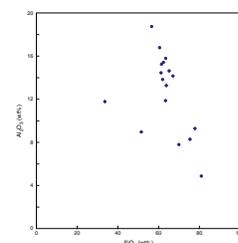
Lower Campanian–Upper Paleocene (Unit 3)

Sedimentology

At Site 1276, this interval is dominated by reddish mudrocks comprising ~80% of the succession, with the remainder being mainly carbonates. These sediments are interpreted as mainly mud turbidites, with a decreasing abundance of carbonate grainstones downhole in the unit (Shipboard Scientific Party, 2004). Shipboard TOC values are relatively low (<2 wt%). Shipboard XRD revealed the presence of quartz, calcite, plagioclase, K-feldspar (including sanidine in Core 210-1276A-32R), common smectite and kaolinite, illite, and local opal in the form of scattered opal-CT lepispheres. The Cretaceous/Cenozoic boundary was identified in interval 210-1276A-21R-4, 41–49 cm, but did not include fine-grained background sediments suitable for sampling during this work. The continuing abundance of smectite is again suggestive of sediment supply from a warm, humid, deeply weathered landmass (Chamley et al., 1979).

Within the central North Atlantic Ocean the entire Turonian to Paleocene time interval is dominated by reddish sediments defined as the Plantagenet Formation (Jansa et al., l979). The succession at Site 1276 is generally similar to the Plantagenet Formation; however, the Site 1276 equivalent of the lower part of this formation (i.e., Unit 4) is sandier than it is elsewhere throughout the central North Atlantic (Jansa et al., 1979; Wise et al., 1986; Gradstein et al., 1990). The sandy nature and ubiquitous red color may be related to the effects of abyssal circulation following the establishment of a deep-marine connection with the South Atlantic Ocean (Tucholke and Vogt, 1979).

Geochemistry

Interelement relationships are shown in Figures F12, F13, and F14, combined with Unit 4, as described above. The relatively few samples of fine-grained sediments from this time interval reflect continuing deposition on a well oxidized seafloor, as suggested by occasional very high values of MnO (up to 0.73 wt%). In addition, significant silica productivity is suggested by relatively high values of SiO_2 (up to 80.13 wt%). Opal was detected by shipboard XRD. P_2O_5 is also relatively enriched (up to 0.33 wt%.), as are Ce, Y, and Nb, elements that are typically associated with phosphate in deep-sea sediments. An apatite phase is to be expected in these samples but was not detected by shipboard XRD, possibly because of low absolute abundances.

Regional Comparisons

At Site 398, during early Paleocene–Campanian time, deposition was dominated by reddish brown mudstones, together with reddish marly chalks, marlstone and claystone, and occasional siliciclastic turbidites (Maldonado, 1979). Minor opaline silica is present.

Upper Paleocene–Middle Eocene (Unit 2)

Sedimentology

The sediments that accumulated during this interval are more calcareous than the sediments below (Shipboard Scientific Party, 2004). At Site 1276, >60% of the succession is calciturbidites and the remaining

40% is mudrocks (claystones and mudstones). Colors are mainly sub-dued reddish, grayish, and greenish. Mudrocks become less abundant uphole and colors change to dark reddish brown in places, suggesting an increase in bottom water oxygen content at times. Mudstones are mostly massive and are interpreted as mainly muddy turbidites. Sedi-ments that were reddish at the time of deposition have been patchily reduced to greenish colors during diagenesis, producing a mottled or blotchy appearance. Shipboard TOC values are variable. Shipboard XRD revealed the presence of quartz, plagioclase, alkaline feldspar, local opal-A, opal-CT, and occasional abundant clinoptilolite. Like the under-lying succession, shipboard XRD showed that smectite is abundant together with kaolinite, chlorite, mixed-layer clays, minor illite, and rare possible palygorskite. Clay mineralogy suggests a continuing warm humid climate in the source area (Chamley, 1989). Also, the relatively elevated silica content in some of the mudrocks (up to 72.96 wt%) sug-gests relatively high primary organic productivity coupled with silica diagenesis.

Several interbedded calcareous sandstones contain felsic to mafic vol-canic detritus. This material is assumed to have undergone gravity transport by turbidity currents. One possible source area is the vicinity of the Newfoundland Seamounts (see Pe-Piper et al., 1990), generally to the south, although this may not be consistent with the limited pale-ocurrent evidence from Site 1276 that suggests a turbidite source on the Grand Banks (**Hiscott,** this volume). Regional comparisons suggest that volcanism around the Paleocene/Eocene boundary (~60 Ma) was quite widespread around the North Atlantic (**Marsaglia et al.,** this volume), and thus it is likely that additional, still unknown volcanic centers exist.

In addition to the routine sampling (1 sample every ~10 m; i.e., 5 samples in this interval) 10 additional samples were taken from the up-per Paleocene–middle Eocene interval to determine whether a signifi-cant volcanogenic (i.e., tuffaceous) component is present within the fine-grained background sediments. This might be similar to the com-position of volcaniclastic sediments that were identified at sea within the interbedded sandstone turbidites (Shipboard Scientific Party, 2004; **Marsaglia et al.,** this volume).

An additional feature of this interval is that carbonate grains include numerous very large benthic foraminifers, together with planktonic for-aminifers. Postcruise studies indicate the existence of one or more car-bonate banks within the source area of the redeposited carbonates. Tropical–subtropical communities of organisms with Caribbean affini-ties existed on these build-ups during the latest Paleocene–earliest middle Eocene (Cores 210-1276A-15R to 7R). These carbonates accumulated during the early Eocene climatic optimum, a time of high sea level and global warmth. It is likely that biogeographic provinces moved north-ward at this time, possibly related in part to the development of a "proto–Gulf Stream" (R. Hiscott, pers. comm., 2006; M. Leckie, pers. comm., 2007)

Geochemistry

Analyzed samples are mainly rich in $CaCO_3$, as shown by shipboard determinations, and correspondingly rich in CaO (up to 35.37 wt%), as shown in Table **T1.** This composition reflects an abundance of fine-grained calcareous turbidites that accumulated during late Paleocene–middle Eocene time. The noncalcareous component of these sediments is largely terrigenous, similar in composition to the underlying sedi-

ments, as shown in Figure F15. Volcaniclastic input was observed in the sand fraction using the optical microscope and occurs within interbedded terrigenous turbidites (Shipboard Scientific Party, 2004; Marsaglia et al., this volume). If volcaniclastic sediment is also present in the fine-grained samples that were analyzed (i.e., as fine-grained turbidites or air-fall tuff), these should show higher absolute values of TiO_2 and lower ratios of, for example, terrigenous constituents vs. TiO_2 than the typically terrigenous compositions of fine-grained sediments elsewhere in the cored interval. The crossplot of Al_2O_3 vs. TiO_2 (Fig. F16) shows that this does indeed appear be the case, although mixing with terrigenous sediment has produced a scattered pattern.

In the upper Paleocene–middle Eocene section, the episodic high SiO_2 values can again be attributed to biogenic productivity and subsequent silica diagenesis. The crossplot of Al_2O_3 vs. SiO_2 (Fig. F17), however, suggests that biogenic and terrigenous sediment are mixed. Occasional relatively elevated values of P_2O_5 (up to 5.18 wt%) may also record high organic productivity and related diagenesis. Occasional high values of trace metals (e.g., Ni at 557 ppm) correlate with thin dark layers that are relatively enriched in TOC.

Regional Comparisons

Sediments comparable to those recovered at Site 1276 are present at Site 398 (Sibuet, Ryan, et al., 1979). There, fine-grained calcareous sediments become more oxidized uphole, and subdued green and gray colors give way to reddish colors. Biogenic silica is relatively abundant (20–30 wt%) compared to Site 1276, which is interpreted to reflect enhanced upwelling along the eastern margin of the North Atlantic Ocean basin (e.g., von Breymann et al., 1992). Elsewhere on the Iberia margin more proximal carbonate turbidites were recovered (e.g., ODP Sites 900, 1067, and 1068) (Sawyer, Whitmarsh, Klaus, et al., 1994; Beslier, Whitmarsh, Wallace, and Girardeau, 2001).

Elsewhere, markedly siliceous sediments accumulated widely throughout the central North Atlantic during the early to middle Eocene and are defined as the Bermuda Rise Formation. These sediments are locally very rich in biogenic silica and are commonly siliceous claystone and chert, together with calcareous mudstone. The chert includes isotropic silica (opal-CT) and chalcedonitic quartz. Fine-grained sediments analyzed from DSDP Site 534 in the Blake Bahama Basin are strongly enriched in silica (up to 74.69 wt%) (Robertson, 1983). The siliceous sediments are generally interpreted to reflect a period of high organic productivity (Jansa et al., 1979; Gradstein et al., 1990).

Middle to Upper Eocene (Unit 1)

Sedimentology

Only a small number of samples were taken from this interval. The succession is ~85% mudrocks, consisting of a mixture of mudstone and claystone, together with subordinate calciturbidites (Shipboard Scientific Party, 2004). Subdued brownish colors predominate. Radiolarians were identified in the lower middle Eocene interval. This was the only part of the succession other than the Paleocene in which radiolarians were identified (Shipboard Scientific Party, 2004). Whole-rock XRD revealed quartz, minor plagioclase, common opal-A, and rare zeolite (in Cores 210-1276A-6R and 5R), together with illite and chlorite. The pre-

F15. K_2O vs. TiO_2, Unit 2, p. 36.
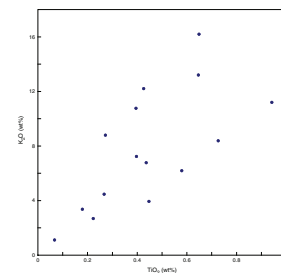
F16. Al_2O_3 vs. TiO_2, Unit 2, p. 37.
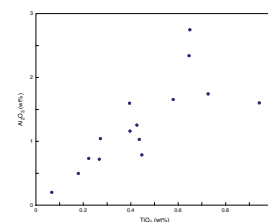
F17. SiO_2 vs. TiO_2, Unit 2, p. 38.
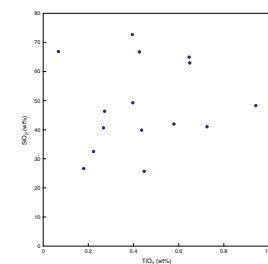
dominance of illite and chlorite is consistent with derivation of terrigenous sediments from a landmass undergoing erosion in a temperate climate with little chemical weathering (Chamley, 1989). This contrasts with the previous period when weathering took place in a warm humid setting and carbonate build-ups occurred in shallow water.

Shipboard TOC values are somewhat variable. Visual diagenetic features include small carbonate concretions and reduction haloes. Shipboard optical petrographic study of the coarser silt and sand fraction revealed widespread siliceous cement, opal-CT lepispheres, and minor chalcedonitic quartz.

Geochemistry

The chemical composition of the fine-grained terrigenous sediment component appears similar to the underlying succession (Table T1). A crossplot of Al_2O_3 vs. TiO_2 (Fig. F18) supports this dominantly terrigenous input, although one sample is relatively enriched in TiO_2. Occasional relatively high absolute values of CaO (up to 6.61 wt%) record the fine-grained component of calciturbidites derived from the shallower margin above the CCD. Some high values of SiO_2 (up to 67.97 wt%) also point to significant productivity of biogenic silica plus the effects of silica diagenesis, as indicated by shipboard smear slide and XRD studies. MnO values are unusually low compared to the underlying Cenozoic part of the succession (<380 ppm). This, in part, reflects dilution by the abundant fine-grained carbonate; however, it is also possible that diagenetic conditions were relatively reducing during the middle to late Eocene time of high carbonate input, promoting dissolution and mobility of manganese. Occasional slightly higher values of trace metals (e.g., Ni at 102 ppm) may again reflect an association with organic matter, as seen in Unit 2.

Regional Comparisons

The background hemipelagic sediments at Site 1276 are noncalcareous and accumulated below the CCD, although rapidly deposited calciturbidites appear in this interval (Fig. F3). Background hemipelagic sediments similar to those at Site 1276, defined as the Blake Ridge Formation, accumulated throughout the central North Atlantic from middle Eocene to Pliocene time (Tucholke and Vogt, 1979; Jansa et al., 1979; Sheridan, Gradstein, et al., 1983). By contrast, at Site 398 on the Iberia margin mainly pelagic carbonates accumulated above the CCD with a greater abundance of siliciclastic and carbonate turbidites than at Site 1276 (Maldonado, 1979). Only the fine-grained sediments that were analyzed from successive 10-m depth intervals are included in the depth vs. composition plots, and the additional samples analyzed from Unit 2 (at closely spaced intervals) were used to determine whether a volcaniclastic component is present or excluded (see above).

Sources of Fine-Grained Sediment

To summarize the results outlined above and highlight changes through time, abundances of selected major element oxides and trace elements were plotted against depth in meters below seafloor (Figs. F19–F38). Unit boundaries are indicated in these plots (see also Fig. F3).

Major element oxides that are associated with terrigenous constituents, as already discussed, show an overall uphole decrease in absolute

F18. Al_2O_3 vs. TiO_2, Unit 1, p. 39.
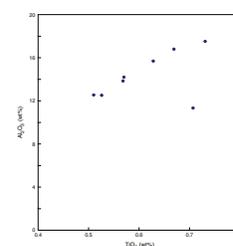
abundances, as illustrated for Al_2O_3 (Fig. **F19**), TiO_2 (Fig. **F20**), K_2O (Fig. **F21**), and Fe_2O_3 (Fig. **F22**). These constituents are mainly associated with detrital clay minerals (Chamley et al., l979). In addition to shipboard XRD analysis of clay minerals, more specialized postcruise XRD studies revealed that from the base of the hole to ~1550 mbsf only illite-smectite mixed-layer minerals, some more exotic mixed-layers, kaolinite, illite, and chlorite exist (T. Pletsch, pers. comm., 2006). From 1550 mbsf, there is a very rapid upward increase in smectite from 0% to ~50%, corresponding to the lower levels of Subunit 5B (1550–1500 mbsf). Smectite makes up 60%–80% of the clay minerals in Subunit 5A and probably remains dominant above this, although a postcruise study of clay minerals higher in the succession was not carried out.

Silica shows an overall increase in abundance uphole (Fig. **F23**), which suggests an increase of an independent constituent, probably biogenic silica, as noted earlier. Very high values of silica, locally seen in the upper part of the succession, are related to occurrences of opaline silica as determined by XRD and smear slides. The pelagic component is low in carbonate (Fig. **F24**) except where resedimented by turbidity currents because the site was continuously below the CCD. Some carbonate (e.g., siderite) formed diagenetically within the sediments. P_2O_5 (Fig. **F25**) is higher in the upper Cretaceous (Campanian) and Cenozoic parts of the succession, which could relate to primary productivity variations, as noted earlier. MnO (Fig. **F26**) exhibits low values with occasional "spikes" that probably relate to penecontemporaneous precipitation of ferromanganese oxides when seafloor conditions were strongly oxidizing. These spikes occur in reddish Turonian–Paleogene sediments (Units 4 and 3). Some MnO spikes in the Albian (Subunit 5b) may relate to accumulation at times when the seafloor was more oxidizing because these sediments are well burrowed in contrast to those above and below.

MgO shows an upward decrease, followed by high values in Unit 3 and then a decrease in Units 2 and 1 (Fig. **F27**). The abundance in Unit 3 correlates with elevated values of Al_2O_3, K_2O, MnO, P_2O_5, Ni, Cr, Cu, Zn, La, Sr, Y, and Zr (Table **T1**). These samples show a relative enrichment in an authigenic phase (i.e, phosphate) and a detrital phase (i.e., smectite rich). These sediments are well oxidized and accumulated on a current-influenced seafloor. Deep-sea currents may have carried in fine-grained detrital sediment from an area of contrasting provenance or clay mineral composition, which would explain the high values of MgO in Unit 3.

By contrast, Na_2O (Fig. **F28**) shows an uphole increase in abundance, which generally correlates with a measured downhole decrease in the porosity of clays and silts (Shipboard Scientific Party, 2004). The trend in Na_2O can be attributed to the expulsion of salt water during compaction and burial because Na_2O values have not been corrected for salt content. Otherwise, Na_2O would be expected to correlate with lithogenous constituents (e.g., sodium feldspar) and have an uphole decrease as in Figures **F19, F20, F21,** and **F22.**

Of the trace elements, Rb shows an uphole decrease in abundance (Fig. **F29**) like the terrigenous-derived major element oxides shown in Figures **F19, F20, F21,** and **F22.** Some other trace elements also show a general uphole decrease in abundance, including Cr (Fig. **F30**), Ni (Fig. **F31**), Zn (Fig. **F32**), V (Fig. **F33**), Ba (Fig. **F34**), and Zr (Fig. **F35**). Ni and Zn are weakly enriched in organic-rich layers, especially those in Unit 5 of Albian–Turonian age. Cu (Fig. **F36**) and Ce (Fig. **F37**) show little downhole variation but have much higher values locally near the

F19. Al_2O_3 vs. depth, p. 40.
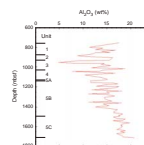
F20. TiO_2 vs. depth, p. 41.
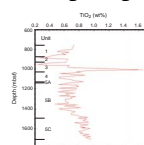
F21. K_2O vs. depth, p. 42.
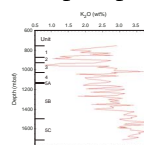
F22. Fe_2O_3 vs. depth, p. 43.
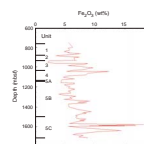
F23. SiO_2 vs. depth, p. 44.
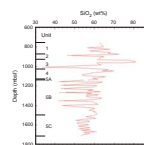
F24. CaO vs. depth, p. 45.
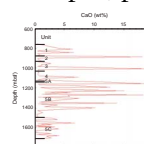
F25. P_2O_5 vs. depth, p. 46.
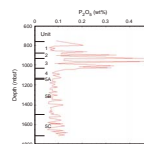
F26. MnO vs. depth, p. 47.
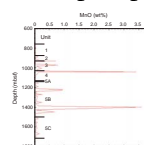
Unit 2/3 boundary. These trace elements are also enriched in manganiferous horizons, as in Unit 4 of Turonian–Santonian age. Ba (Fig. F34) is relatively depleted in pre-Cenomanian sediments but is commonly elevated above this, which may relate to increased primary productivity (Dymond et al., 1992). Y and Ce (Fig. F37) are generally enriched in phosphatic intervals.

The dominantly terrigenous provenance of Site 1276 sediments is also supported by distinctive patterns of shale-normalized plots for representative mudrock samples from each lithologic unit (Fig. F38). These samples are compositionally similar to the North American shale composite (NASC) (Gromet et al., 1984); however, Cr, Zr, and Ba are slightly depleted, whereas Y, La, Ce, Nd, and Sr are slightly enriched. The small deviations from NASC may relate to the concentration of trace elements within authigenic marine phases (e.g., Sr within diagenetic carbonates, Y within marine phosphates, and Ba related to plankton productivity). Variations, however, also reflect the composition of the source region on land, which may differ from the NASC.

Available data from Site 1276 suggest a generally north-northeastward flow of turbidity currents during the Albian with considerable variation (Hiscott, this volume). A possible source of turbidity currents was therefore on the southeastern Grand Banks (i.e., the Avalon Uplift that was exposed at the time) (Hiscott, this volume). The regional geology of the Avalon Uplift includes lithologic equivalents of the Meguma Zone, which consists of lower Paleozoic rocks that were metamorphosed during the late Paleozoic Alleghenian orogeny, where they are exposed in Nova Scotia (Schenk, l995; Williams et al., l995). Other parts of the Grand Banks correlate with the Precambrian to lower Paleozoic Avalon Zone and its Carboniferous cover of mainly sandstones and shales (e.g., Jansa and Wade, 1975; Williams et al., 1995; Sanford et al., 1979). White micas that were dated from Cretaceous sandstones at Site 1276 by the Ar/Ar method have mainly yielded ages of 260–340 Ma (Carboniferous–Permian) characteristic of the Alleghenian orogeny. In addition, a smaller number of samples have older ages (400–600 Ma) characteristic of the Acadian orogeny. These results suggest that a possible source area of Cretaceous sediments at Site 1276 was the Meguma Zone under the southern Grand Banks, assuming that the Meguma rocks there experienced Alleghenian metamorphism (Wilson and Hiscott, this volume). However, it is also possible that an exotic terrane of Hercynian metamorphic rocks, similar to those of western Europe, is present in the Grand Banks area and contributed sediment to Site 1276. A wide variety of rocks exposed in Newfoundland and on the Grand Banks, potentially including the lower Paleozoic Meguma Group, its upper Paleozoic sedimentary cover, Devonian/Carboniferous granites and granodiorites, and even an exotic Hercynian terrane may have contributed fine-grained sediment to Site 1276.

In summary, overall downhole trends of major element oxides and trace elements are consistent with deposition on a subsiding rifted passive margin on which the relative abundance of land-derived lithogenous constituents gradually decreased with time relative to the amount of pelagic, biogenic, and authigenic constituents. The geochemical evidence also suggests that the composition of the predominantly terrigenous component at Site 1276 remained relatively constant during the Albian–Santonian (Units 4 and 5) but may have become more variable subsequently when deep-sea currents became more active.
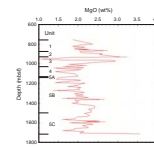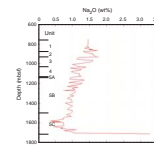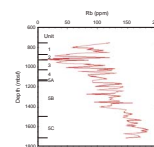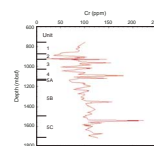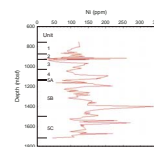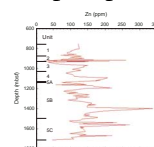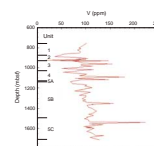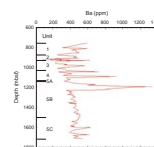
Origin of Black Shales

Organic-rich sediments of the Albian–Turonian interval (Unit 5) are time equivalents of black shales within the Hatteras Formation of the central North Atlantic (Jansa et al., l979; Tucholke et al., l989; Arthur et al., l987; Hofmann et al., 2001; **Arnaboldi and Meyers,** this volume). However, the Albian succession at Site 1276 is greatly expanded because of a high input of sediments from turbidity currents. Numerous organic-rich horizons that do not coincide with known OAEs are present low in the Albian succession.

The lowest example of well-recognized black shales is from the middle of lithologic Subunit 5C, of early Albian age, and could represent OAE 1b, known as the "Paquier" event. Higher in Subunit 5C, an organic-rich interval that is characterized by terrestrially derived kerogen could correspond to OAE 1c (Shipboard Scientific Party, 2004). Dark layers near the base of Subunit 5B might represent a presently unrecognized OAE-type layer. The top of Subunit 5B, of late Albian age, may correspond to OAE 1d, which is known to be dominated by terrigenous organic matter elsewhere (see Hofmann et al., 2001; Leckie et al., 2002). An organic-rich interval in the middle of Subunit 5A is likely to represent the "mid-Cenomanian event" (Leckie et al., 2002). The organic-rich layer at the top of lithologic Subunit 5A, of late Cenomanian–earliest Turonian age, probably corresponds to OAE 2, the "Bonarelli" event. In addition, several minor organic-rich layers occur within the overlying succession.

Many of the dark gray to black layers show an enrichment in organic carbon, commonly >2 wt% plus a few very high values (>5 wt%) based on shipboard analysis (Shipboard Scientific Party, 2004). Postcruise TOC determinations confirm the presence of organic matter enrichment in these layers, but TOC in most of the sediments is lower (mainly <2 wt%) (**Arnaboldi and Meyers,** this volume). Shipboard analysis also revealed low hydrogen index (HI) values (HI < 100 mg HC/g TOC) and C/N ratios averaging ~20, suggesting a strong influence of terrestrially derived organic matter. A positive correlation between C/N ratios and TOC contents also supports a terrigenous origin for the sedimentary organic matter. Maximum temperature (T_{max}) values of <435° were consistently determined postcruise using the Rock-Eval 7 method, significantly less than shipboard measurements (Pletsch and Cramer, 2006; Pletsch et al., 2006). The only exceptions occur within 5 m of the upper alkaline basalt sill near the base of the hole. Much of the kerogen present in the sediments could have been derived from reworked, previously altered terrestrial components, as confirmed by vitrinite reflectance studies (Pross et al., 2007).

In a related postcruise geochemical study, **Arnaboldi and Meyers** (this volume) provide chemical analyses of 30 black shales from the Turonian, Cenomanian–Turonian, Cenomanian, Albian–Cenomanian and Albian intervals for the major element oxides Al_2O_3, TiO_2, Fe_2O_3, MgO, and K_2O and the trace elements Ba, Cd, Cr, Cu, Mo, Re, U, V, and Zn. The trends of Al, Ti, Fe (partially), K, and Mg support a dominantly terrigenous input. Cr, Cu, V, and Zn are slightly enriched in the black shales, as is Ba, a possible paleoproductivity indicator. For Zr, however, only three measured values exceed those of the adjacent background sediments (i.e., one from the Albian–Cenomanian interval [338 ppm] and two from the Albian interval [480 and 548 ppm]). Uranium values reach a high of 9.6 ppm in the Albian, and the Albian also exhibits the highest Cd values (7.51 ppm), with Rh values reaching 0.301 ppm and
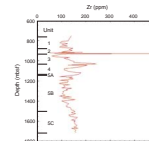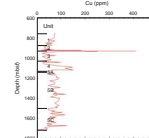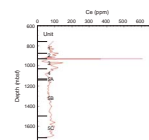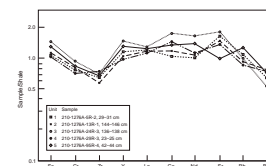
Mo values reaching 181 ppm. In general, these additional geochemical data support deposition and diagenesis of the black shales in dysoxic to anoxic settings (**Arnaboldi and Meyers,** this volume).

The relative inputs of terrestrial vs. marine organic matter within the black shales can be assessed using a combination of C/N ratios, N isotopes, C isotopic ratios, and determinations of kerogen type. However, even with all this evidence, unambiguous discrimination of the sources of organic matter in the Cretaceous black shales remains difficult and must take account of organic-matter diagenesis during burial (e.g., Arthur, l979; Arthur et al., l987; Meyers et al., l984; Meyers, l994; Wise et al., l986; Hofmann et al., 2001). Presently available evidence from Site 1276 suggests that OAE 2 and 1b contain dominantly marine organic matter, whereas OAE 1c contains mainly terrestrial organic carbon. Few data exist for OAE 1d, but a mainly marine origin for the organic carbon is possible (Shipboard Scientific Party, 2004; **Arnaboldi and Meyers,** this volume).

CONCLUSIONS

The following conclusions are made concerning the origin of the fine-grained sediments cored at Site 1276, moving forward through time.

1. The Albian–Turonian interval shows a strong terrigenous input, consistent with very high sedimentation rates and the results of petrographic studies of interbedded coarser grained sediments. Background pelagic and hemipelagic sedimentation was continuously beneath the calcite compensation depth during the Albian–Eocene time interval. Localized high concentrations of iron and carbonate reflect the formation of siderite concretions. Redox sensitive elements (e.g., Cu, V, Ni, and Zn) are associated with organic-rich layers (black shales) of variably mixed terrigenous and marine origin.
2. The Turonian–Santonian time interval records the accumulation of reddish sediments within a strongly oxidizing deep-marine setting, probably following the establishment of deep-water connections between the South Atlantic and North Atlantic basins. Manganese oxide and trace metals (e.g., Cu, Ni, and Pb) were coprecipitated from seawater on a strongly oxidizing seafloor.
3. During the Campanian to late Paleocene, moderate upwelling along the Newfoundland margin gave rise to relatively high organic productivity, as reflected in a modest enrichment in silica, phosphate, and associated trace elements (e.g., Ce and Y). Local Mn enrichment coupled with reddish color of sediments suggests that the seafloor generally remained well oxidized during this time interval.
4. During the late Paleocene to middle Eocene, background deposition was still influenced by relatively high productivity, as suggested by locally high phosphate and silica contents and evidence of silica diagenesis. However, primary productivity was lower than it was on the conjugate Iberia margin, as recorded at Site 398.
5. During the middle Eocene, background marine productivity remained relatively high. These sediments are more reducing, as suggested by commonly gray-green subdued colors and low

manganese contents. Fine-grained deposition was dominated by input of calcareous turbidites during this time, associated with the development of shallow-marine carbonate build-ups in the source area.

6. Chemical composition of the dominantly terrigenous input at Site 1276 remained relatively constant from the Aptian to Eocene and corresponds quite closely to the average composition of terrigenous shale (NASC). This, in turn, suggests that these sediments are well mixed, consistent with an origin as fine-grained turbidites and hemipelagic sediments.

7. A volcaniclastic contribution was found in the sand turbidites of late Paleocene–middle Eocene age and appears also to be present in the fine-grained size fraction of this time interval, mixed with terrigenous sediment.

8. The mudrocks were sourced in the adjacent continental margin of Newfoundland and the Grand Banks (e.g., the Avalon Uplift area) from a number of potential source rocks of different ages, metamorphism, and tectonic affinities.

ACKNOWLEDGMENTS

REFERENCES

Arthur, M.A., 1979. North Atlantic Cretaceous black shales: the record at Site 398 and a brief comparison with other occurrences. *In* Sibuet, J.-C., Ryan, W.B.F., et al., *Init. Repts. DSDP,* 47 (Pt. 2): Washington, DC (U.S. Govt. Printing Office), 719–751. **doi:10.2973/dsdp.proc.47-2.136.1979**

Arthur, M.A., Schlanger, S.O., and Jenkyns, H.C., 1987. The Cenomanian–Turonian oceanic anoxic event, II. Palaeoceanographic controls on organic-matter production and preservation. *In* Brooks, J., and Fleet, A.J. (Eds.), *Marine Petroleum Source Rocks.* Geol. Soc. Spec. Publ., 26:401–420.

Beslier, M.-O., Whitmarsh, R.B., Wallace, P.J., and Girardeau, J. (Eds.), 2001. *Proc. ODP, Sci. Results,* 173: College Station, TX (Ocean Drilling Program). **doi:10.2973/odp.proc.sr.173.2001**

Chamley, H., 1979. North-Atlantic clay sedimentation and palaeoenvironment since the Late Jurassic. *In* Talwani, M., Hay, W., and Ryan, W.B.F. (Eds), *Deep Drilling Results in the Atlantic Ocean: Continental Margins and Paleoenvironment.* Maurice Ewing Ser., 3:342–361.

Chamley, H., 1989. *Clay Sedimentology:* Berlin (Springer-Verlag).

Chamley, H., and Debrabant, P., 1984. Paleoenvironmental history of the North Atlantic region from mineralogical and geochemical data. *Sedimentology,* 40:151–167.

Chamley, H., Debrabant, P., Foulon, J., Giroud d'Argoud, G., Latouche, C., Maillet, N., Maillot, H., and Sommer, F., 1979. Mineralogy and geochemistry of Cretaceous and Cenozoic Atlantic sediments off the Iberian peninsula (Site 398, DSDP Leg 47B). *In* Sibuet, J.-C., Ryan, W.B.F., et al., *Init. Repts. DSDP,* 47 (Pt. 2): Washington, DC (U.S. Govt. Printing Office), 429–449. **doi:10.2973/dsdp.proc.47-2.111.1979**

de Graciansky, P.C., and Chenet, P.Y., 1979. Sedimentological study of cores 138 to 56 (upper Hauterivian to middle Cenomanian): an attempt at reconstruction of paleoenvironments. *Init. Repts. DSDP,* 47 (Part 2): Washington, DC (U.S. Govt. Printing Office), 403–418. **doi:10.2973/dsdp.proc.47-2.109.1979**

Dymond, J., Suess, E., and Lyle, M., 1992. Barium in deep-sea sediment: a geochemical proxy for paleoproductivity. *Paleoceanography,* 7:163–181.

Fitton, J.G., Saunders, A.D., Larsen, L.M., Hardarson, B.S., and Norry, M.J., 1998. Volcanic rocks from the southeast Greenland margin at 63°N: composition, petrogenesis, and mantle sources. *In* Saunders, A.D., Larsen, H.C., and Wise, S.W., Jr. (Eds.), *Proc. ODP, Sci. Results,* 152: College Station, TX (Ocean Drilling Program), 331–350. **doi:10.2973/odp.proc.sr.152.233.1998**

Gradstein, F.M., Jansa, L.F., Srivastava, S.P., Williamson, M.A., Bonham-Carter, G., and Stam, B., 1990. Aspects of North Atlantic paleo-oceanography. *In* Keen, M.J. and Williams, G.L. (Eds.), *The Geology of North America* (Vol. 2): *Geology of the Continental Margin of Eastern Canada:* Boulder (Geol. Soc. Am.), 351–389.

Gromet, L.P., Haskin, L.A., Korotev, R.L., and Dymek, R.F., 1984. The "North American shale composite": its compilation, major and trace element characteristics. *Geochim. Cosmochim. Acta,* 48(12):2469–2482. **doi:10.1016/0016-7037(84)90298-9**

Hart, S.R., and Blusztajn, J., 2006. Age and geochemistry of mafic sills, ODP Site 1276, Newfoundland margin. *Chem. Geol.,* 235(3–4):222–237. **doi:10.1016/j.chemgeo.2006.07.001**

Haq, B.U., Hardenbol, J., and Vail, P.R., 1987. Chronology of fluctuating sea levels since the Triassic. *Science,* 235(4793):1156–1167. **doi:10.1126/science.235.4793.1156**

Hofmann, P., Ricken, W., Schwark, L., and, Leythaeuser, D., 2001. Geochemical signature and related climatic-oceanographic processes for early Albian black shales: Site 417D, North Atlantic Ocean. *Cretaceous Res.,* 22(2):243–257. **doi:10.1006/cres.2001.0253**

Jansa, L.F., Enos, P., Tucholke, B.E., Gradstein, F.M., and Sheridan, R.E., 1979. Mesozoic-Cenozoic sedimentary formations of the North American Basin, western North Atlantic. *In* Talwani, M., Hay, W., and Ryan, W.B.F. (Eds.), *Deep Drilling*

Results in the Atlantic Ocean: Continental Margins and Paleoenvironment. Maurice Ewing Ser., 3:1–57.

Jansa, L.F., and Wade, J.A., 1975. Geology of the continental margin off Nova Scotia and Newfoundland. *In* Linden, W.J.M., and Wade, J.A. (Eds.), *Offshore Geology of Eastern Canada* (Vol. 2): *Regional Geology.* Pap.—Geol. Surv. Can., 51–105.

Karner, G.D., and Shillington, D.J., 2005. Basalt sills of the U reflector, Newfoundland Basin: a serendipitous dating technique. *Geology,* 33(12):985–988. doi:10.1130/G21971.1

Leckie, R.M., Bralower, T.J., and Cashman, R., 2002. Oceanic anoxic events and plankton evolution: biotic response to tectonic forcing during the mid-Cretaceous. *Paleoceanography,* 17(3):1041. doi:10.1029/2001PA000623

Maldonado, A., 1979. Upper Cretaceous and Cenozoic depositional processes and facies in the distal North Atlantic continental margin off Portugal, DSDP Site 398. *In* Sibuet, J.-C., Ryan, W.B.F., et al., *Init. Repts. DSDP,* 47 (Pt. 2): Washington, DC (U.S. Govt. Printing Office), 373–402. doi:10.2973/dsdp.proc.47-2.108.1979

McCave, I.N., 1972. Transport and escape of fine-grained sediment from shelf areas. *In* Swift, D.J.P., Duane, D.B., and Pilkey, O.H. (Eds.), *Shelf Sediment Transport: Process and Pattern:* Stroudsburg, PA (Dowden, Hutchinson and Ross), 225–248.

McCave, I.N., 1979. Depositional features of organic-carbon-rich black and green mudstones at DSDP Sites 386 and 387, western North Atlantic. *In* Tucholke, B.E., Vogt, P.R., et al., *Init. Repts. DSDP,* 43: Washington, DC (U.S. Govt. Printing Office), 411–416. doi:10.2973/dsdp.proc.43.110.1979

Meyers, P.A., 1987. Organic-carbon content of sediments and rocks from Deep Sea Drilling Project Sites 603, 604, and 605, western margin of the North Atlantic. *In* van Hinte, J.E., Wise, S.W., Jr., et al., *Init. Repts. DSDP,* 93: Washington, DC (U.S. Govt. Printing Office), 1187–1194. doi:10.2973/dsdp.proc.93.150.1987

Meyers, P.A., 1994. Preservation of elemental and isotopic source identification of sedimentary organic matter. *Chem. Geol.,* 114(3–4):289–302. doi:10.1016/0009-2541(94)90059-0

Meyers, P.A., Brassell, S.C., and Huc, A.Y., 1984. Geochemistry of organic carbon in South Atlantic sediments from DSDP Leg 75. *In* Hay, W.W., Sibuet, J.-C., et al., *Init. Repts. DSDP,* 75: Washington, DC (U.S. Govt. Printing Office), 967–981. doi:10.2973/dsdp.proc.75.129.1984

Pe-Piper, G., Piper, D.J.W., Keen, M.J., and McMillan, N.J., 1990. Igneous rocks of the continental margin: tectonic and geophysical overview. *In* Keen, M.J., and Williams, G.L. (Eds.), *The Geology of North America* (Vol. 2): *Geology of the Continental Margin of Eastern Canada:* Boulder (Geol. Soc. Am.), 75–85.

Pletsch, T., 1997. Clay minerals in Cretaceous deep-water formations of the Rif and the Betic Cordillera (northern Morocco and southern Spain). *Ann., Soc. Geol. Nord,* 26.

Pletsch, T., and Cramer, B., 2006. Overpressure and sill fracturing at ODP Site 1276, Newfoundland margin? *Schriftenr. D. Geowiss.,* 45:135.

Pletsch, T., Pross, J., Kus, J., Scheeder, G., Wehner, H., and Arnaboldi, M., 2006. Hydrocarbon potential of ODP Hole 1276A, the first deep well on Newfoundland margin [paper presented at the ICDP-IODP Colloquium, Greifswald, Germany, 27–29 March 2006].

Pollastro, R.M., 1993. Considerations and applications of the illite/smectite geothermometer in hydrocarbon-bearing rocks of Miocene to Mississippian age. *Clays Clay Miner.,* 41(2):119–133. doi:10.1346/CCMN.1993.0410202

Pross, J., Pletsch, T., Shillington, D.J., Ligouis, B., Schellenberg, F., and Kus, J., 2007. Thermal alteration of terrestrial palynomorphs in mid-Cretaceous organic-rich mudstones intruded by an igneous sill (Newfoundland Margin, ODP Hole 1276A). *Int. J. Coal Geol.,* 70:277–291. doi:10.1016/j.coal.2006.06.005

Robertson, A.H.F. 1983. Latest Cretaceous and Eocene palaeoenvironments in the Blake-Bahama Basin, western North Atlantic. *In* Sheridan, R.E., Gradstein, F.M., et

al., *Init. Repts. DSDP,* 76: Washington, DC (U.S. Govt. Printing Office), 763–780. **doi:10.2973/dsdp.proc.76.138.1983**

Robertson, A.H.F., and Bliefnick, D.M., 1983. Sedimentology and origin of Lower Cretaceous pelagic carbonates and redeposited clastics, Blake-Bahama Formation, Deep Sea Drilling Project Site 534, western equatorial Atlantic. *In* Sheridan, R.E., Gradstein, F.M., et al., *Init. Repts. DSDP,* 76: Washington, DC (U.S. Govt. Printing Office), 795–828. **doi:10.2973/dsdp.proc.76.140.1983**

Sanford, B.V., Grant, A.C., Wade, J.A., and Barss, M.S., 1979. *Geology of Eastern Canada and Adjacent Areas.* Map.—Geol. Surv. Can., 1401A.

Sawyer, D.S., Whitmarsh, R.B., Klaus, A., et al., 1994. *Proc. ODP, Init. Repts.,* 149: College Station, TX (Ocean Drilling Program). **doi:10.2973/odp.proc.ir.149.1994**

Schenk, P.E., 1995. Meguma zone. *In* Williams, H. (Ed.), *The Geology of North America* (Vol. 6): *Geology of the Appalachian–Caledonian Orogen in Canada and Greenland:* Boulder (Geol. Soc. Am.), 261–277.

Sheridan, R.E., Gradstein, F.M., et al., 1983. *Init. Repts. DSDP,* 76: Washington, DC (U.S. Govt. Printing Office). **doi:10.2973/dsdp.proc.76.1983**

Shillington, D.J., Holbrook, W.S., Van Avendonk, H.J.A., Tucholke, B.E., Hopper, J.R., Louden, K.E., Larsen, H.C., and Nunes, G.T., 2006. Evidence for asymmetric non-volcanic rifting and slow incipient oceanic accretion from seismic reflection data on the Newfoundland margin. *J. Geophys. Res.,* 111(B9):B09402. **doi:10.1029/2005JB003981**

Shipboard Scientific Party, 2004. Site 1276. *In* Tucholke, B.E., Sibuet, J.-C., Klaus, A., et al., *Proc. ODP, Init. Repts.,* 210: College Station, TX (Ocean Drilling Program), 1–358. **doi:10.2973/odp.proc.ir.210.103.2004**

Sibuet, J.-C., Ryan, W.B.F., et al., 1979. *Init. Repts. DSDP,* 47 (Pt. 2): Washington, DC (U.S. Govt. Printing Office). **doi:10.2973/dsdp.proc.47-2.1979**

Stow, D.A.V., Huc, A.-Y., and Bertrand, P., 2001. Depositional processes of black shales in deep water. *Mar. Pet. Geol.,* 18(4):491–498. **doi:10.1016/S0264-8172(01)00012-5**

Tucholke, B.E., Austin, J.A., and Uchupi, E., 1989. Crustal structure and rift-drift evolution of the Newfoundland Basin. *In* Tankard, A.J., and Balkwell, H.R. (Eds.), *Extensional Tectonics and Stratigraphy of the North Atlantic Margins.* AAPG Mem., 46:247–263.

Tucholke, B.E., Sibuet, J.-C., Klaus, A., et al., 2004. *Proc. ODP, Init. Repts.,* 210: College Station, TX (Ocean Drilling Program). **doi:10.2973/odp.proc.ir.210.2004**

Tucholke, B.E., and Vogt, P.R., 1979. Western North Atlantic: sedimentary evolution and aspects of tectonic history. *In* Tucholke, B.E., Vogt, P.R., et al., *Init. Repts. DSDP,* 43: Washington, DC (U.S. Govt. Printing Office), 791–825. **doi:10.2973/dsdp.proc.43.140.1979**

von Breymann, M.T., Emeis, K.-C., and Suess, E., 1992. Water depth and diagenetic constraints on the use of barium as a palaeoproductivity indicator. *In* Summerhayes, C.P., Prell, W.L., and Emeis, K.-C. (Eds.), *Upwelling Systems: Evolution Since the Early Miocene.* Geol. Soc. Spec. Publ., 64:273–284.

Williams, H., O'Brien, S.J., King, A.F., and Anderson, M.M., 1995. Avalon zone—Newfoundland. *In* Keen, M.J. and Williams, G.L. (Eds.), *The Geology of North America* (Vol. 2): *Geology of the Continental Margin of Eastern Canada:* Boulder (Geol. Soc. Am.), 226–237.

Wise, S.W., Jr., Van Hinte, J.E., Mountain, G.S., Biart, B.N.M., Covington, J.M., Drugg, W.S., Dunn, D.A., Farre, J., Habib, D., Hart, M.B., Haggerty, J.A., Johns, M.W., Lang, T.H., Meyers, P.A., Miller, K.G., Moullade, M.R., Muza, J.P., Ogg, J.G., Okamura, M., Sarti, M., and von Rad, U., 1986. Mesozoic-Cenozoic clastic depositional environments revealed by DSDP Leg 93 drilling on the continental rise off the eastern United States. *In* Summerhayes, C.P., and Shackleton, N.J. (Eds.), *North Atlantic Palaeogeography.* Geol. Soc. Spec. Publ., 21:35–66.

Figure F1. Bathymetric map showing the location of Site 1276 on the rifted margin of Newfoundland. From Tucholke, Sibuet, Klaus, et al. (2004). Smts. = seamounts.
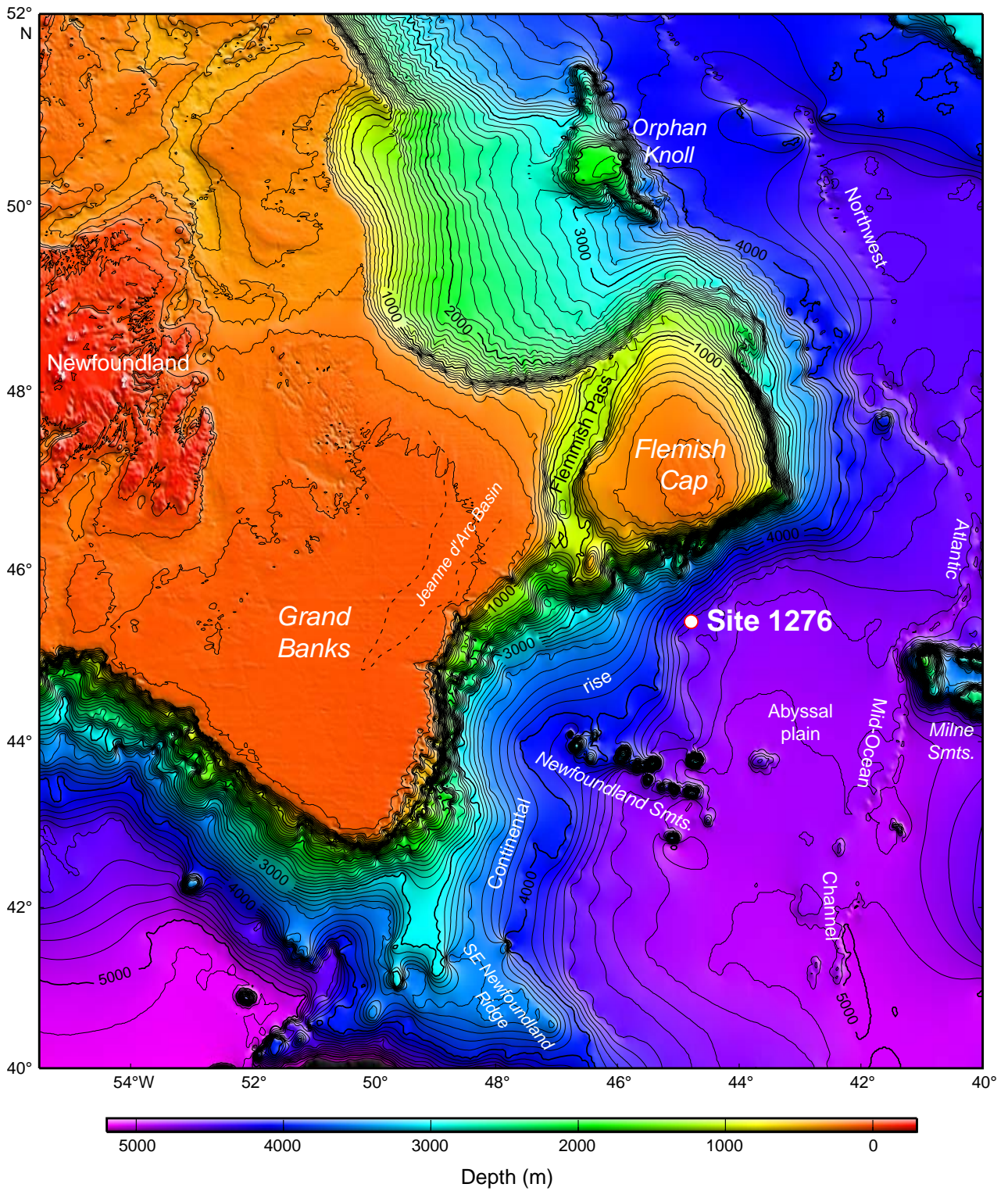
Figure F2. Segments of SCREECH 2 seismic profiles across the continental rise and proximal abyssal plain of the Newfoundland rifted margin. Cored sediments at Site 1276 date to earliest Oligocene to earliest Albian or latest Aptian. The hole did not reach the basement, which is inferred to be >8 m.y. older and at least tens of meters below the deepest core, which terminated in a basaltic sill. From **Tucholke and Sibuet** (this volume).
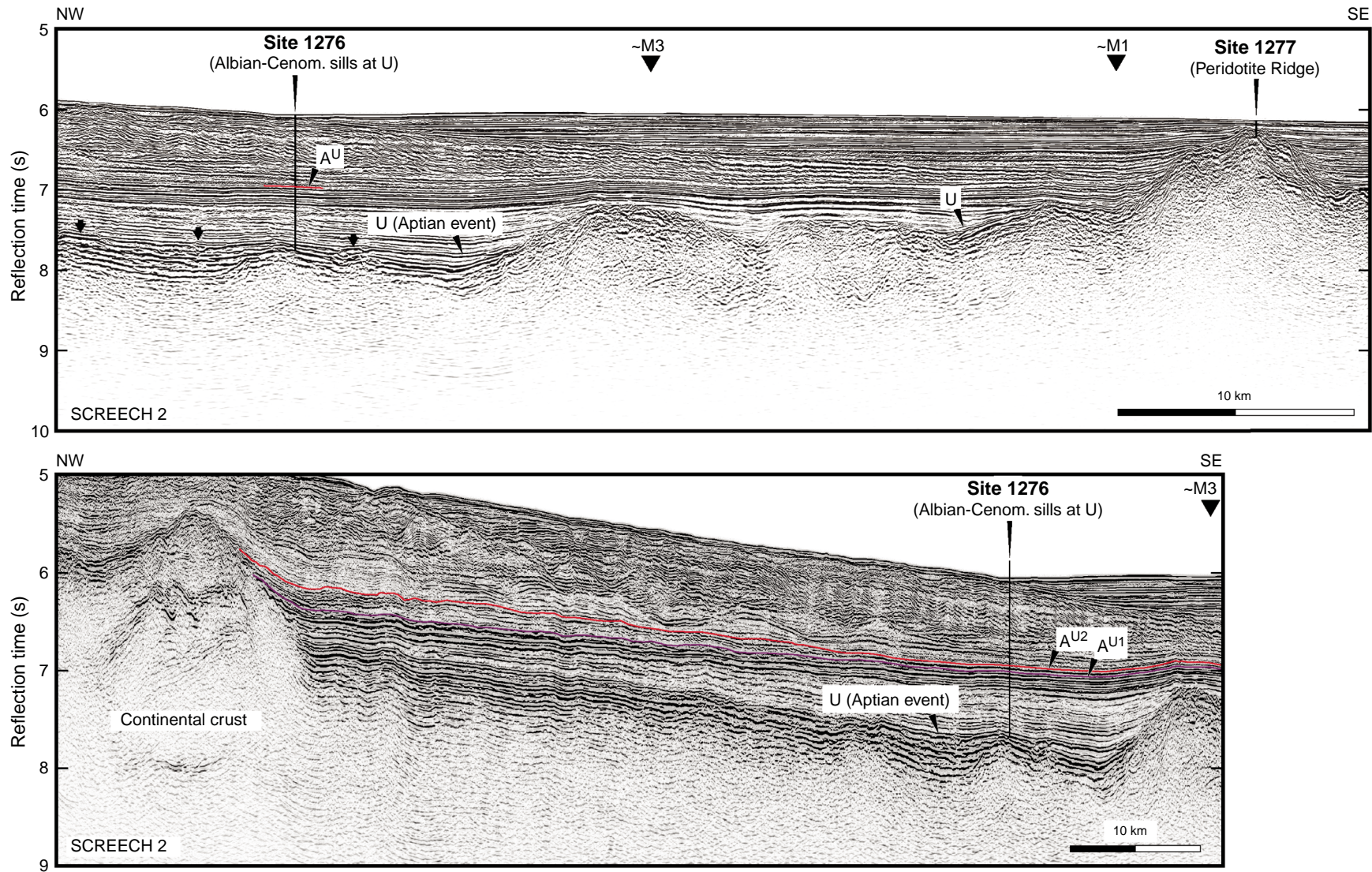
Figure F3. Summary of core recovery, lithology, and depositional processes at Site 1276. Lithology and grain-size columns highlight the role of coarse turbidites but give less information about the interbedded hemipelagic and fine-grained terrigenous sediments that were chemically analyzed during this study. From Tucholke, Sibuet, Klaus, et al. (2004).
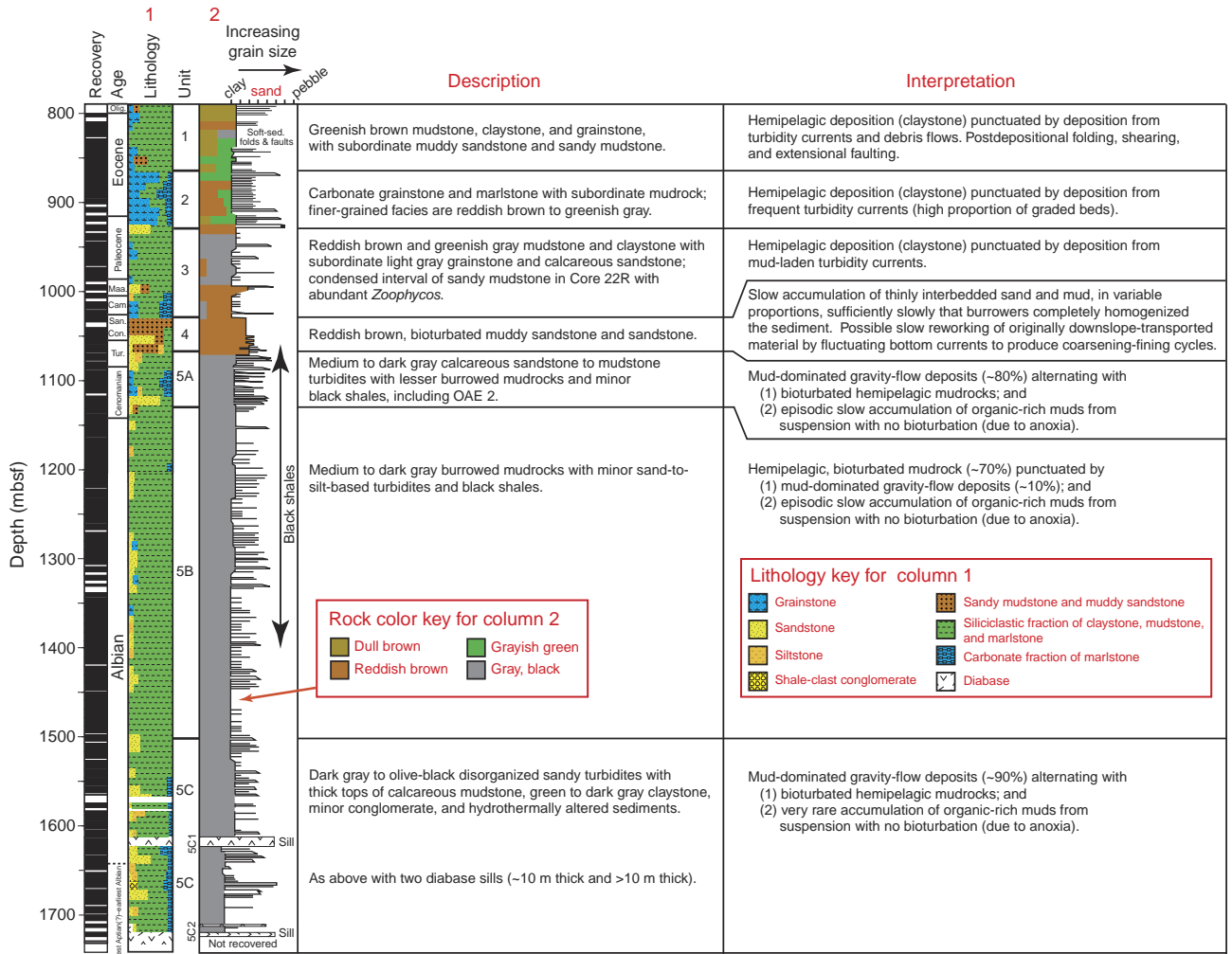
Figure F4. Crossplot of Al_2O_3 vs. K_2O, Unit 5.
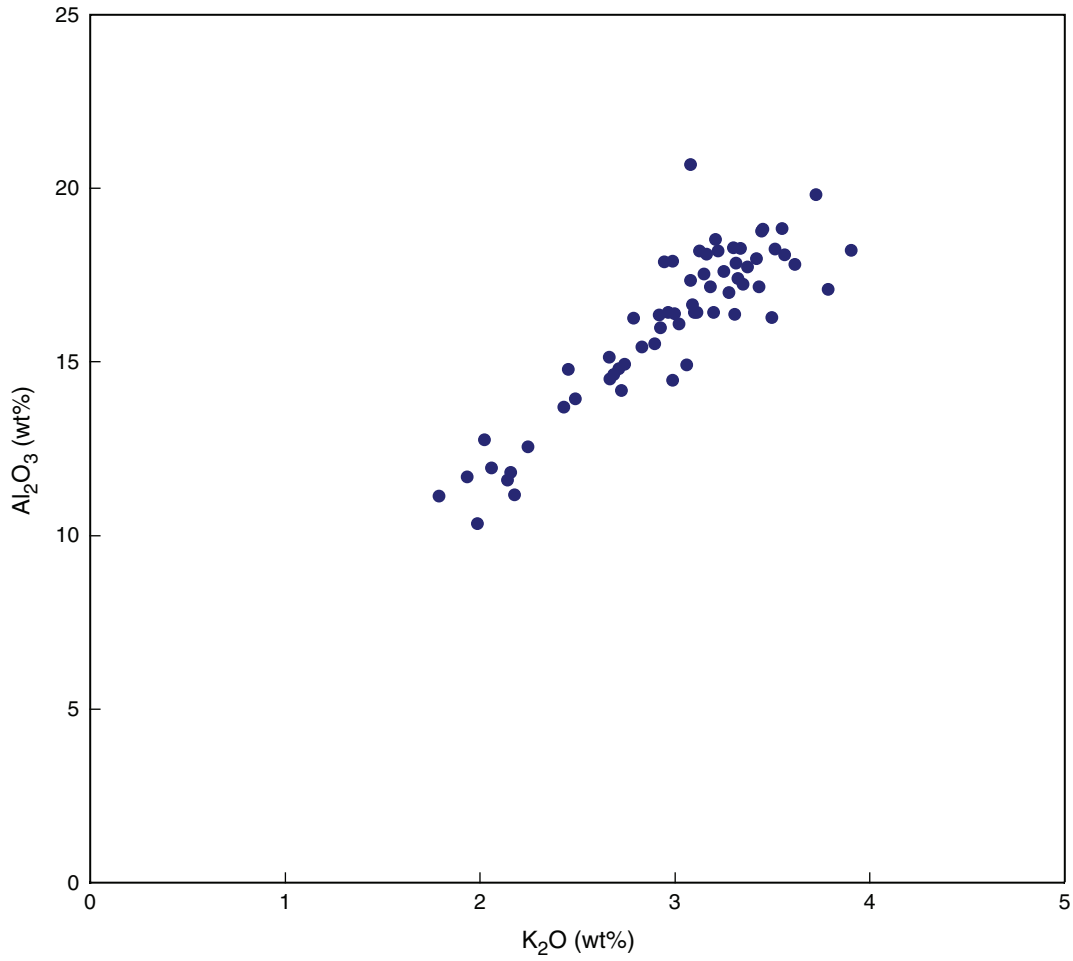
Figure F5. Crossplot of Al_2O_3 vs. MgO, Unit 5.
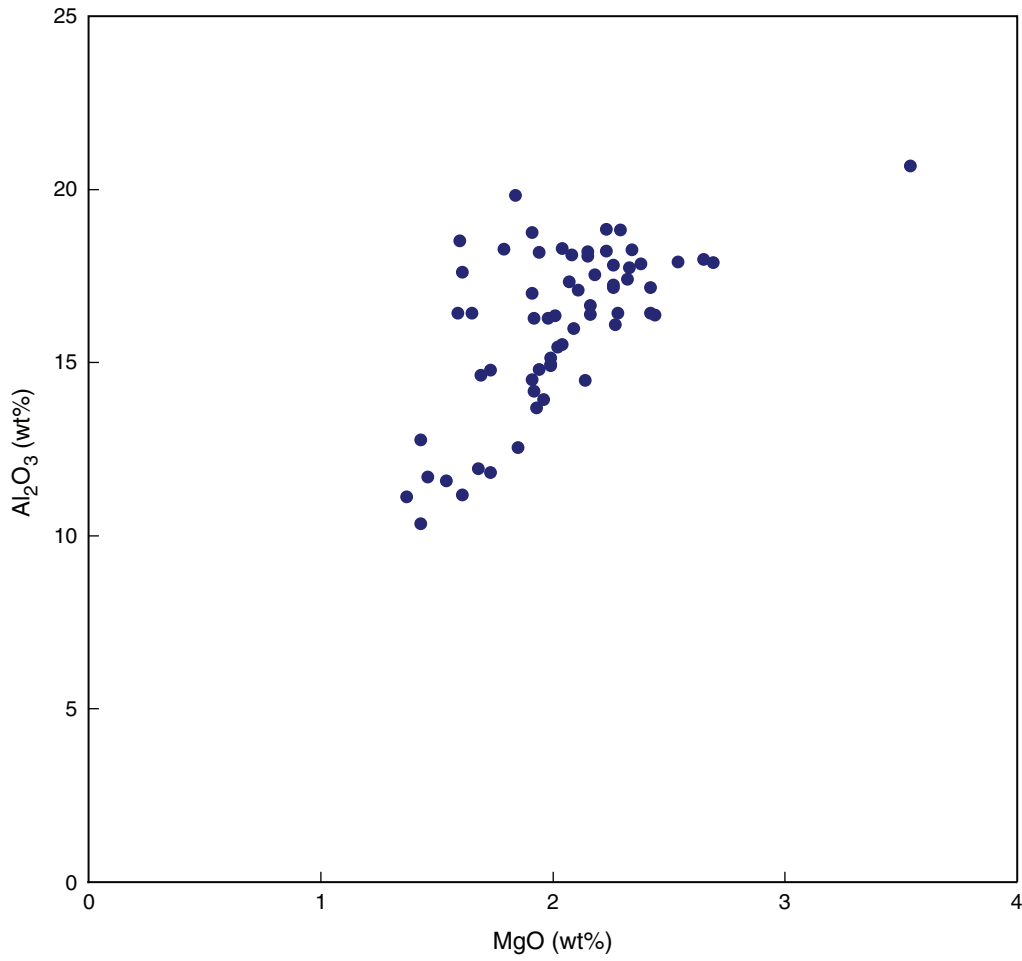
Figure F6. Crossplot of Al_2O_3 vs. Na_2O, Unit 5.
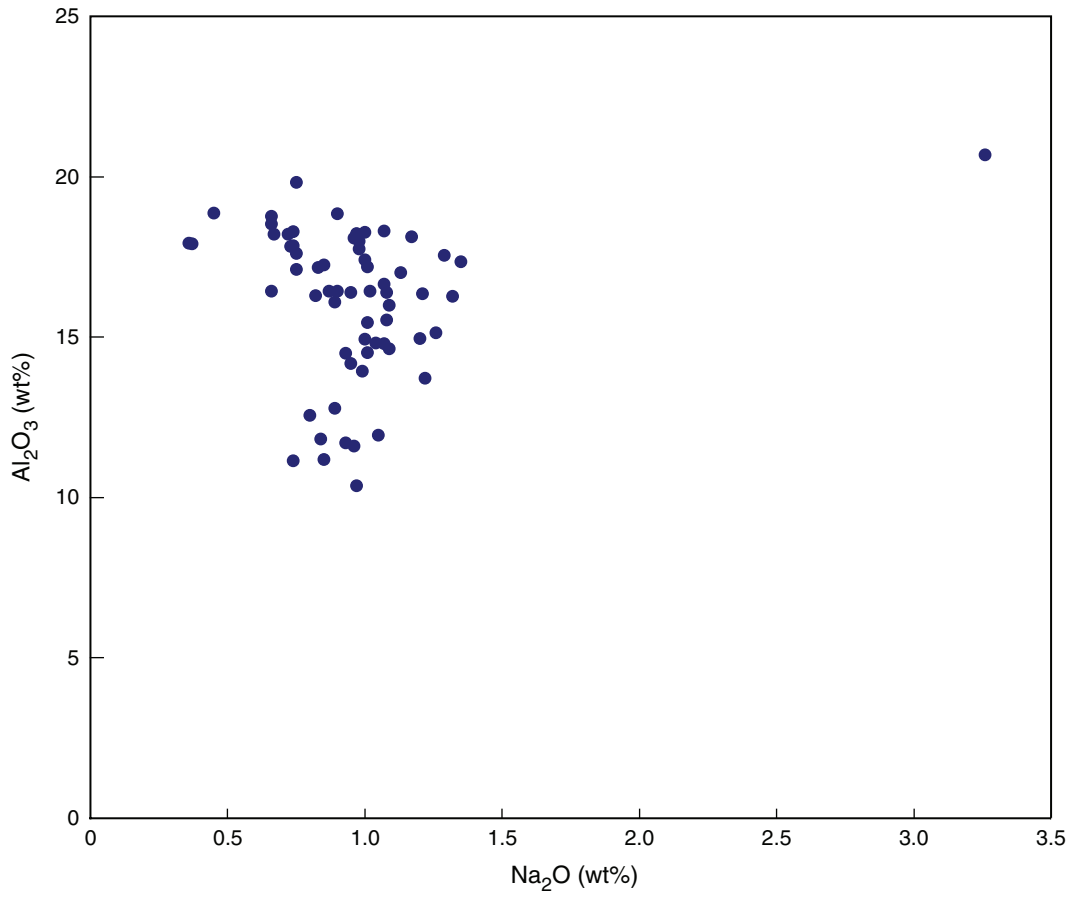
Figure F7. Crossplot of Al_2O_3 vs. TiO_2, Unit 5.
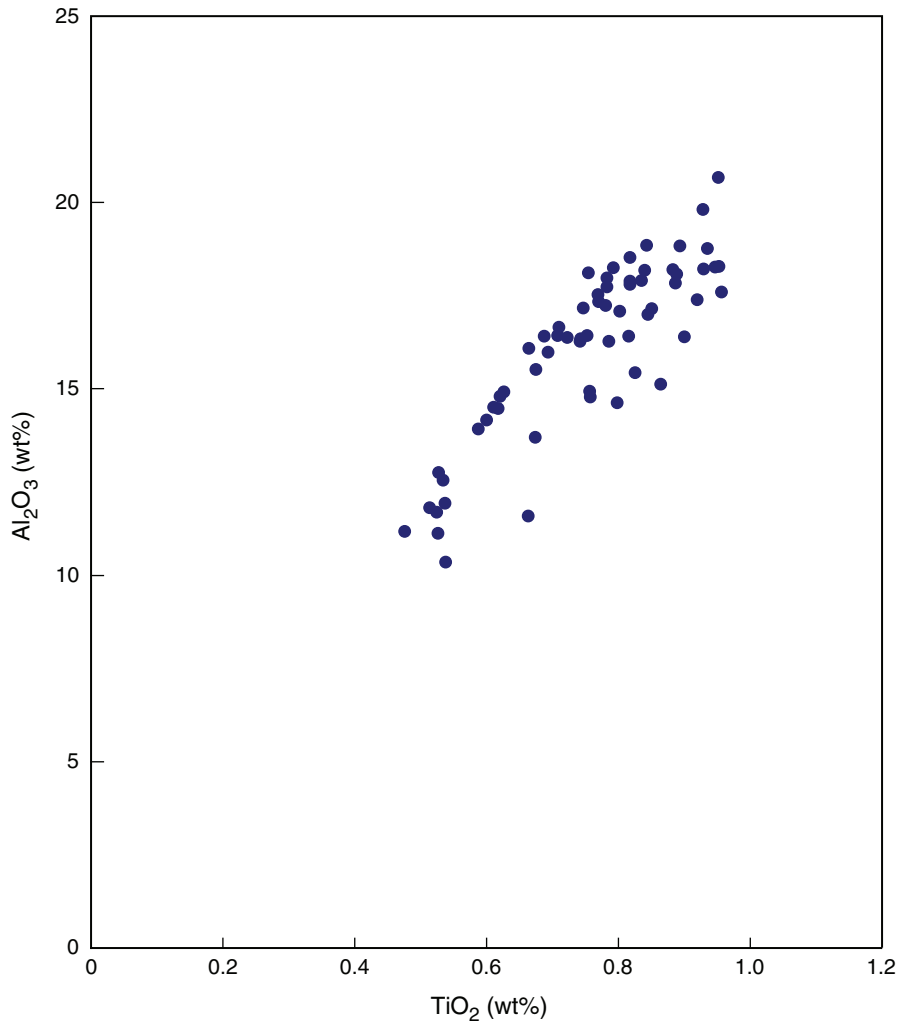
Figure F8. Crossplot of MgO vs.TiO$_2$, Unit 5.
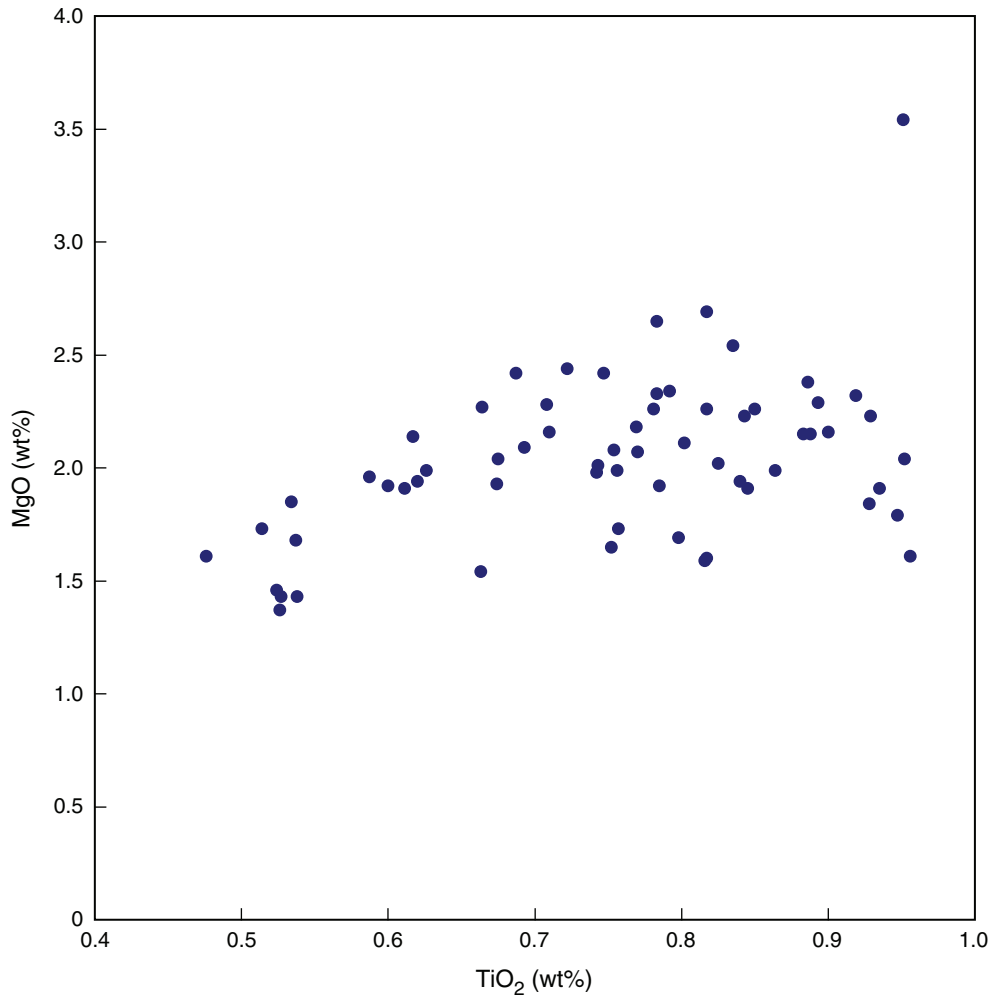
Figure F9. Crossplot of Al_2O_3 vs. Fe_2O_3, Unit 5.
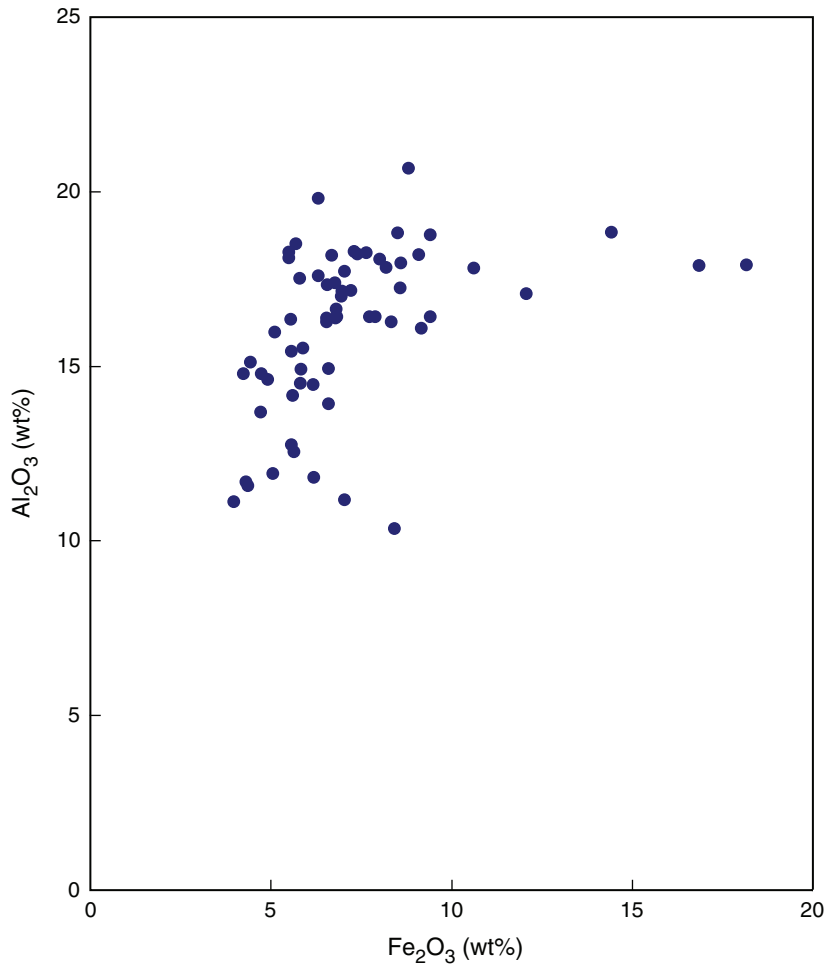
Figure F10. Crossplot of Al_2O_3 vs. SiO_2, Unit 5.
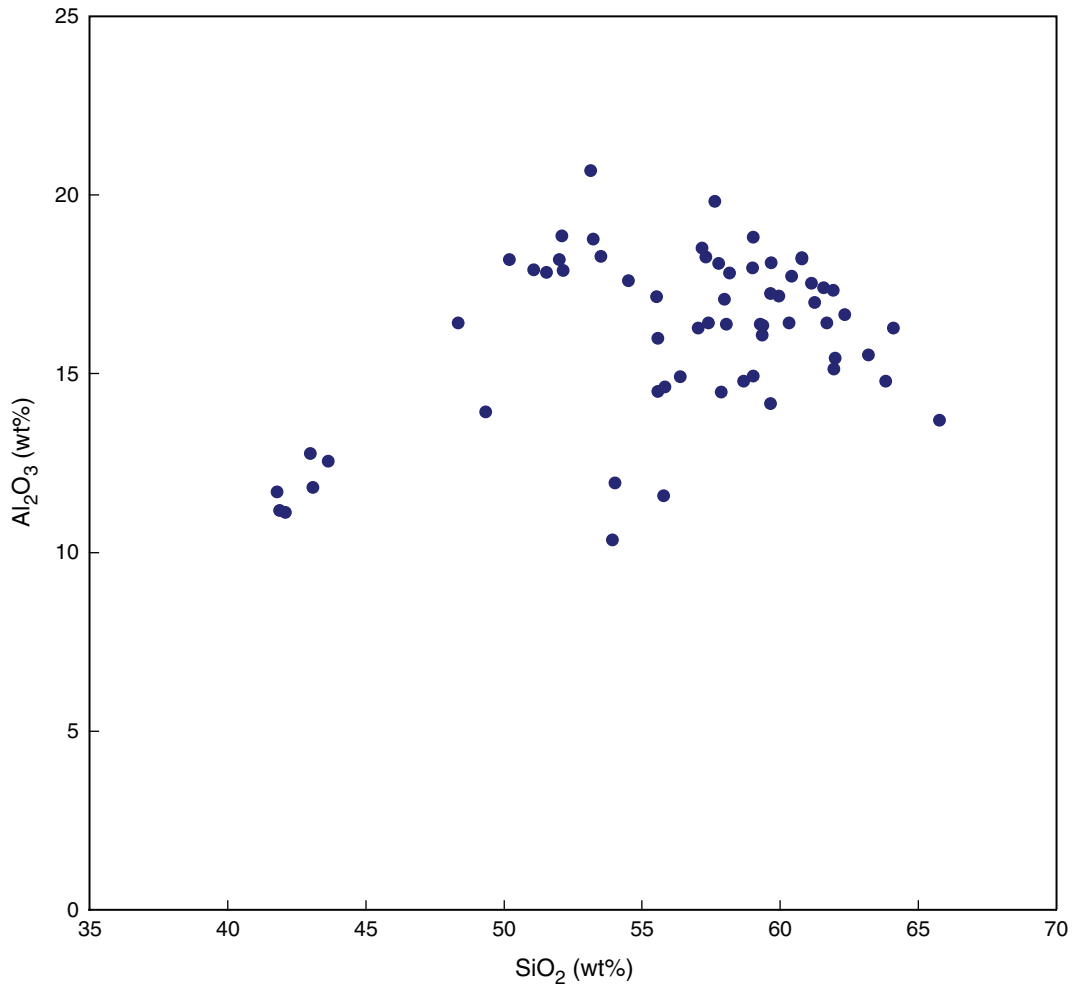
Figure F11. Crossplot of Fe_2O_3 vs. MnO, Unit 5.
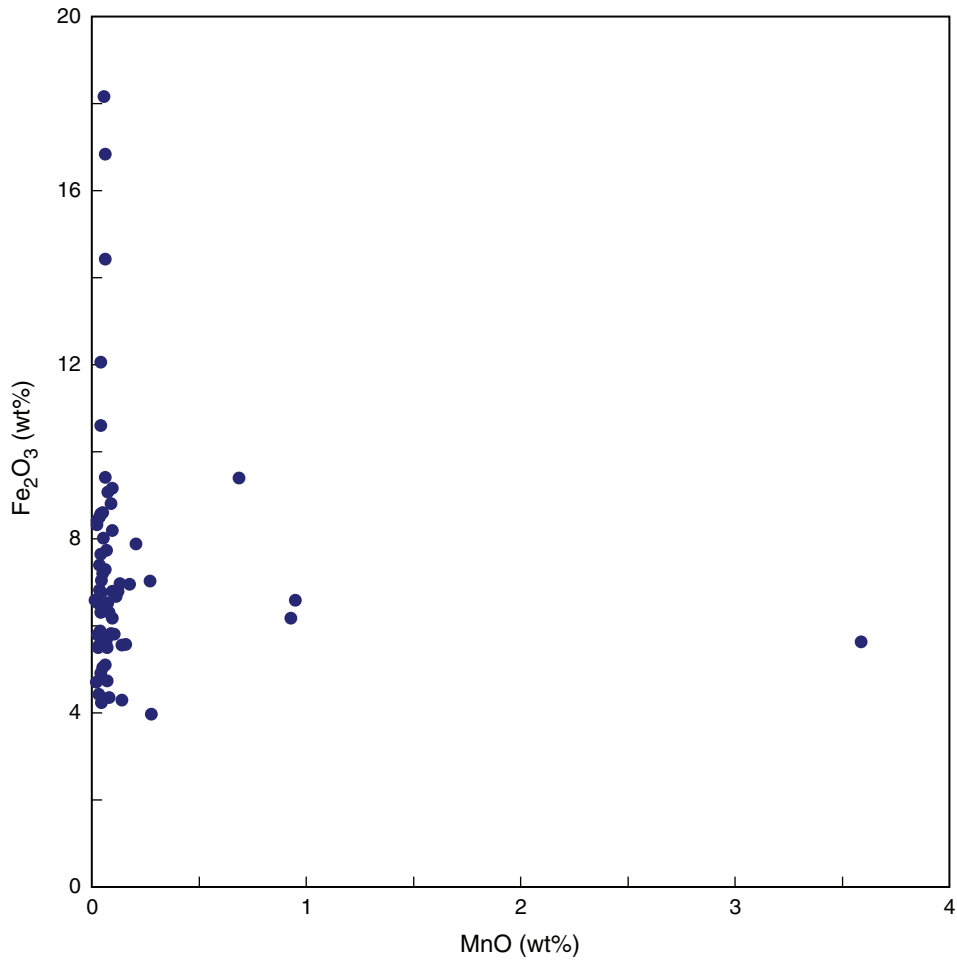
Figure F12. Crossplot of Al_2O_3 vs. TiO_2, Units 3 and 4.
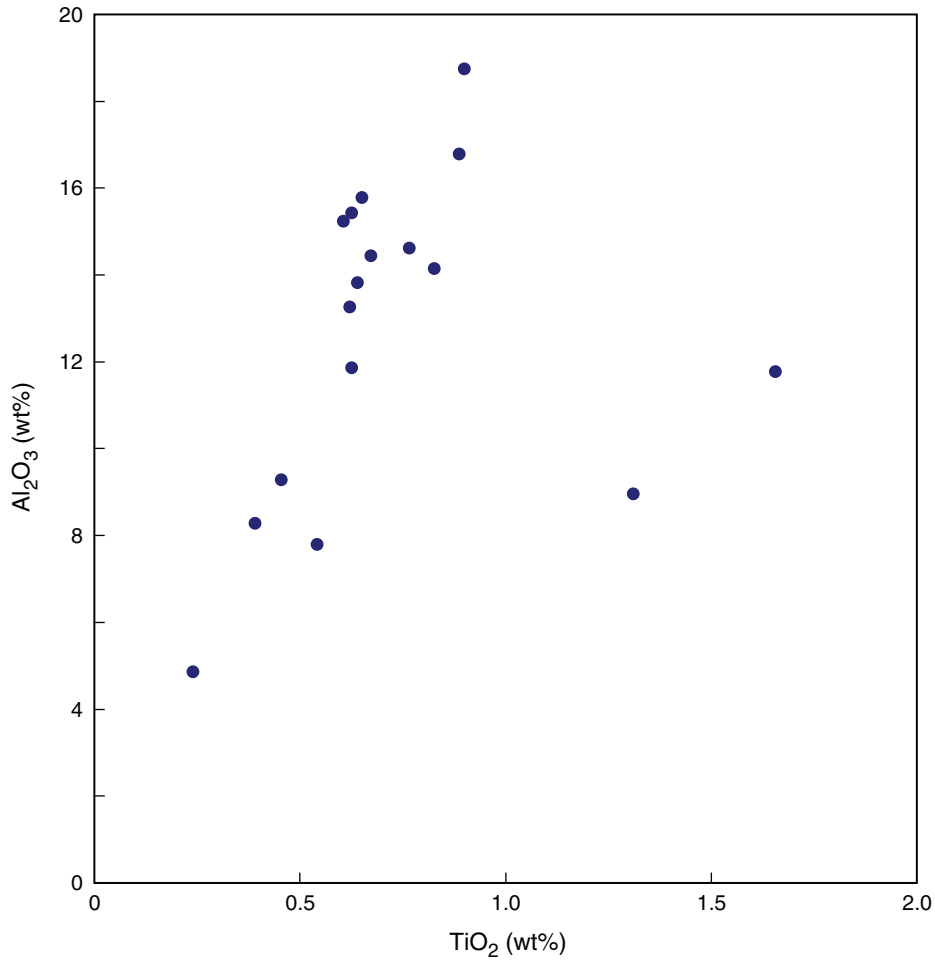
Figure F13. Crossplot of Al_2O_3 vs. K_2O, Units 3 and 4.
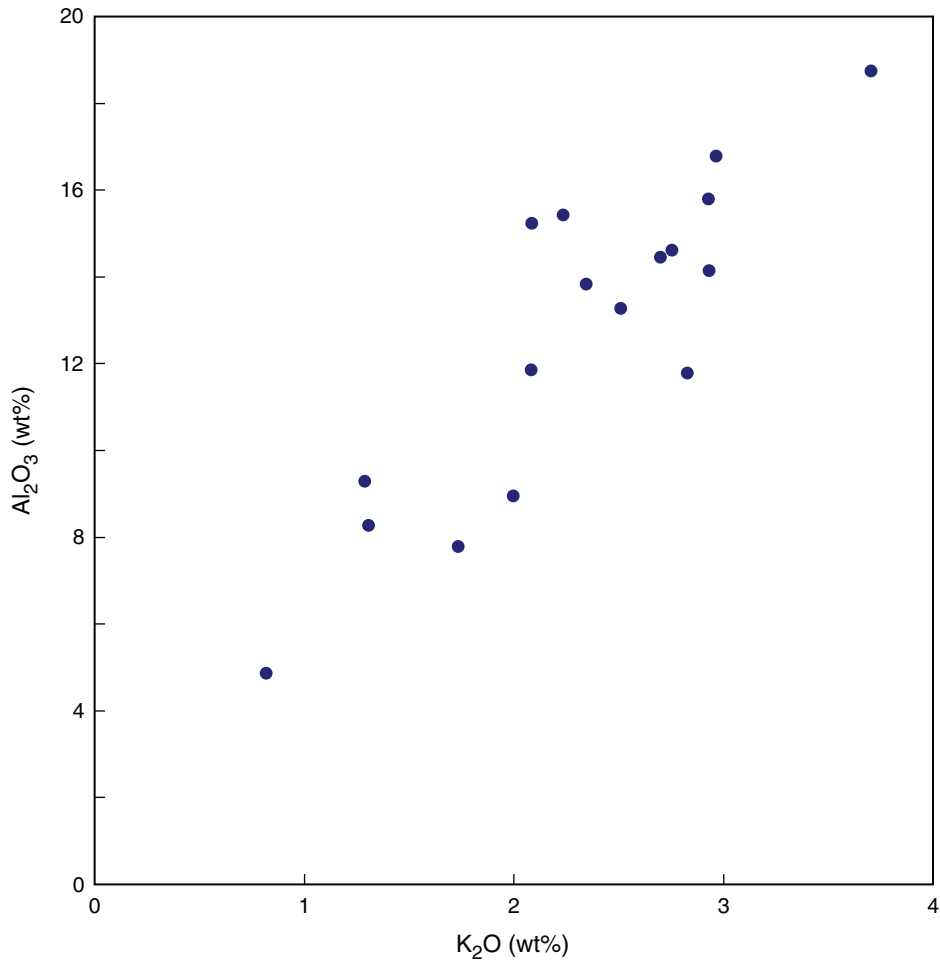
Figure F14. Crossplot of Al_2O_3 vs. SiO_2, Units 3 and 4.
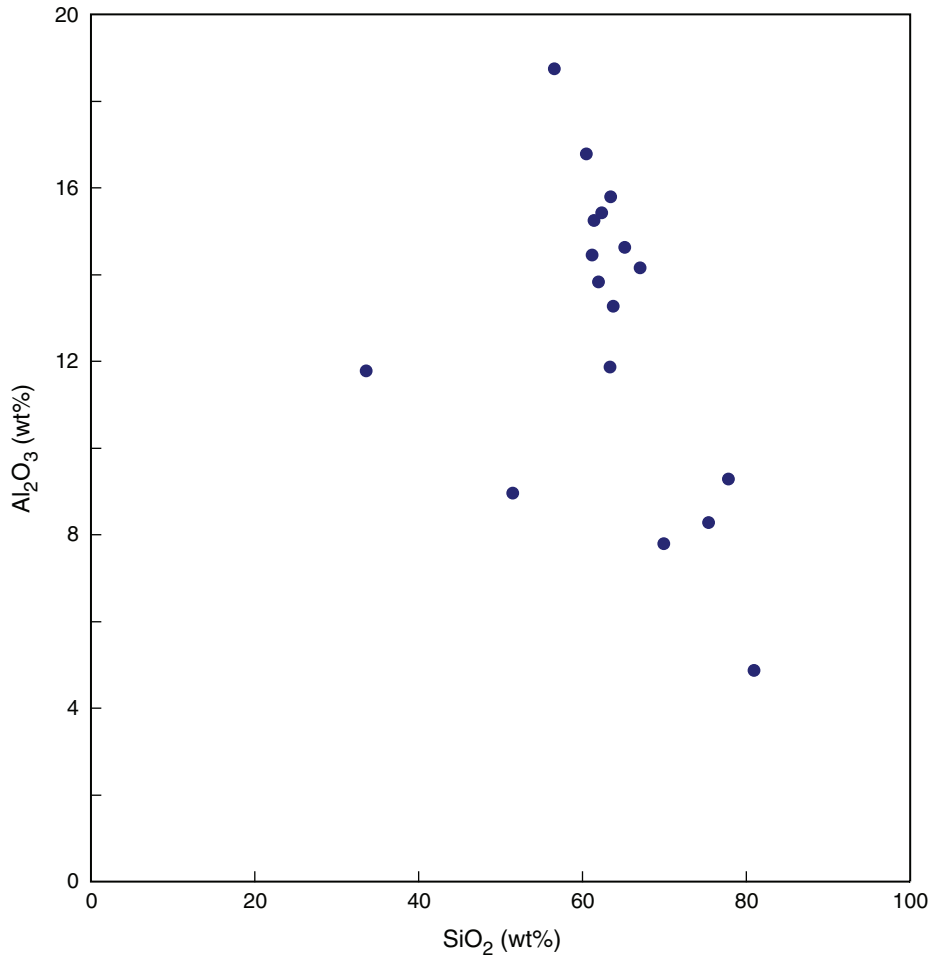
Figure F15. Crossplot of K_2O vs. TiO_2, Unit 2.
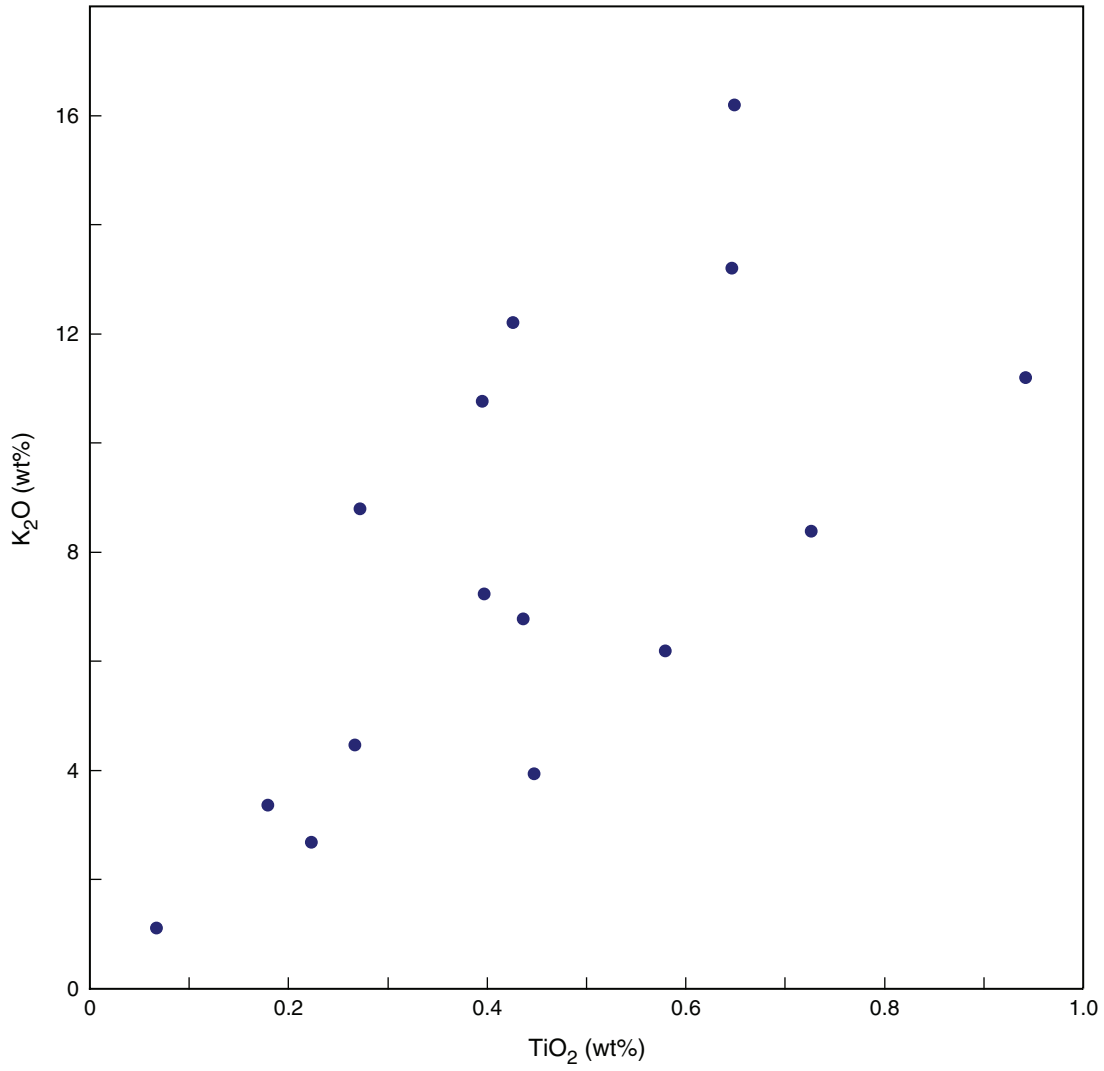
Figure F16. Crossplot of Al_2O_3 vs. TiO_2, Unit 2.
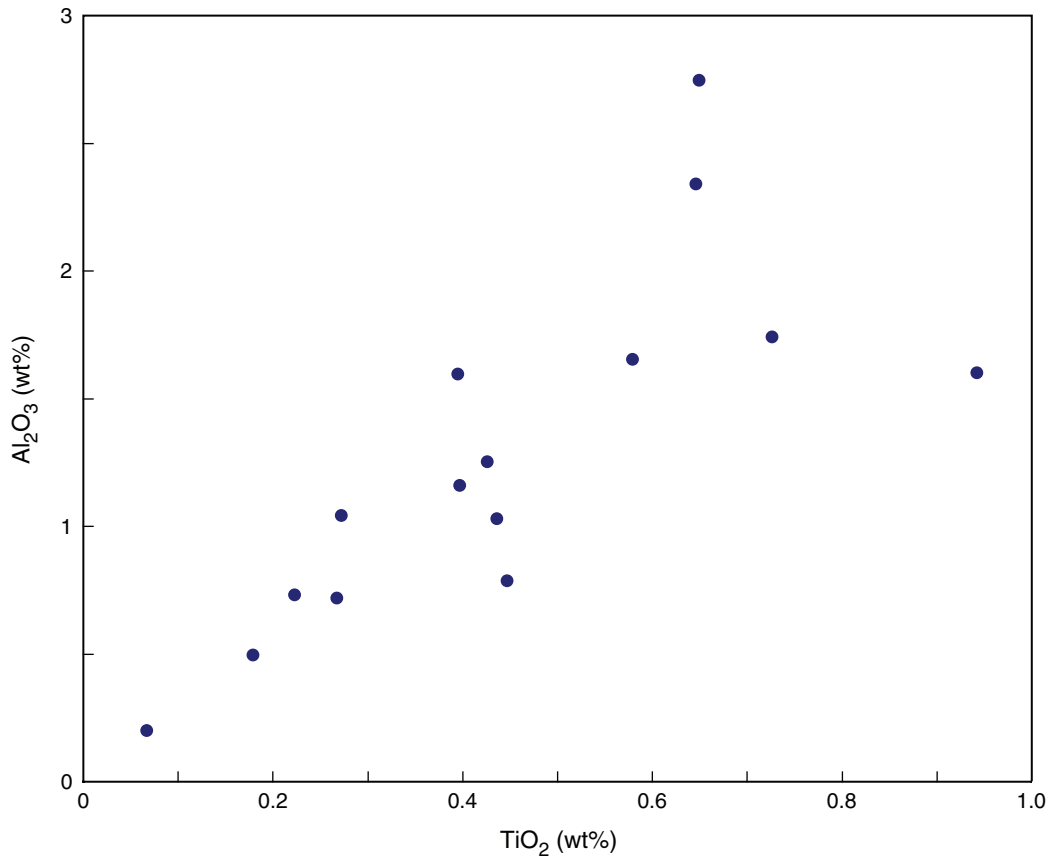
Figure F17. Crossplot of SiO_2 vs. TiO_2, Unit 2.
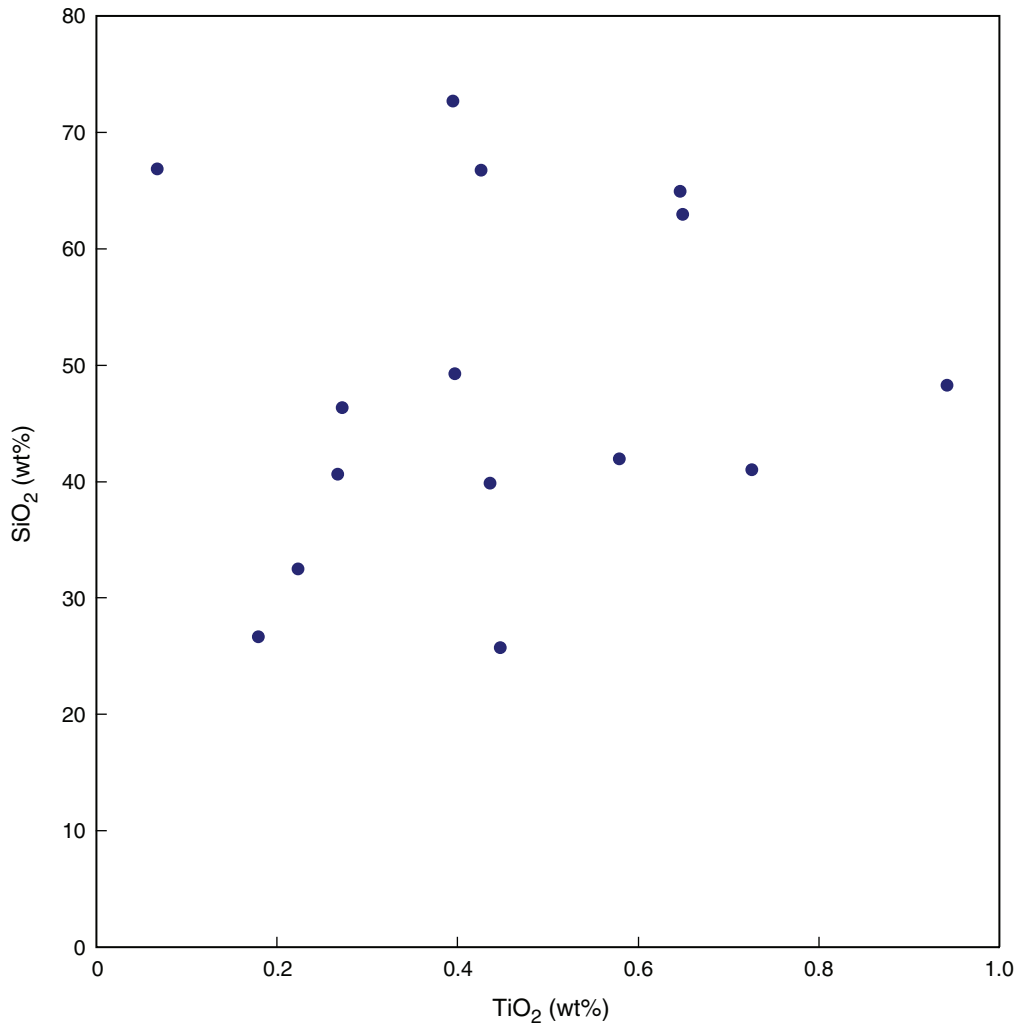
Figure F18. Crossplot of Al_2O_3 vs. TiO_2, Unit 1.
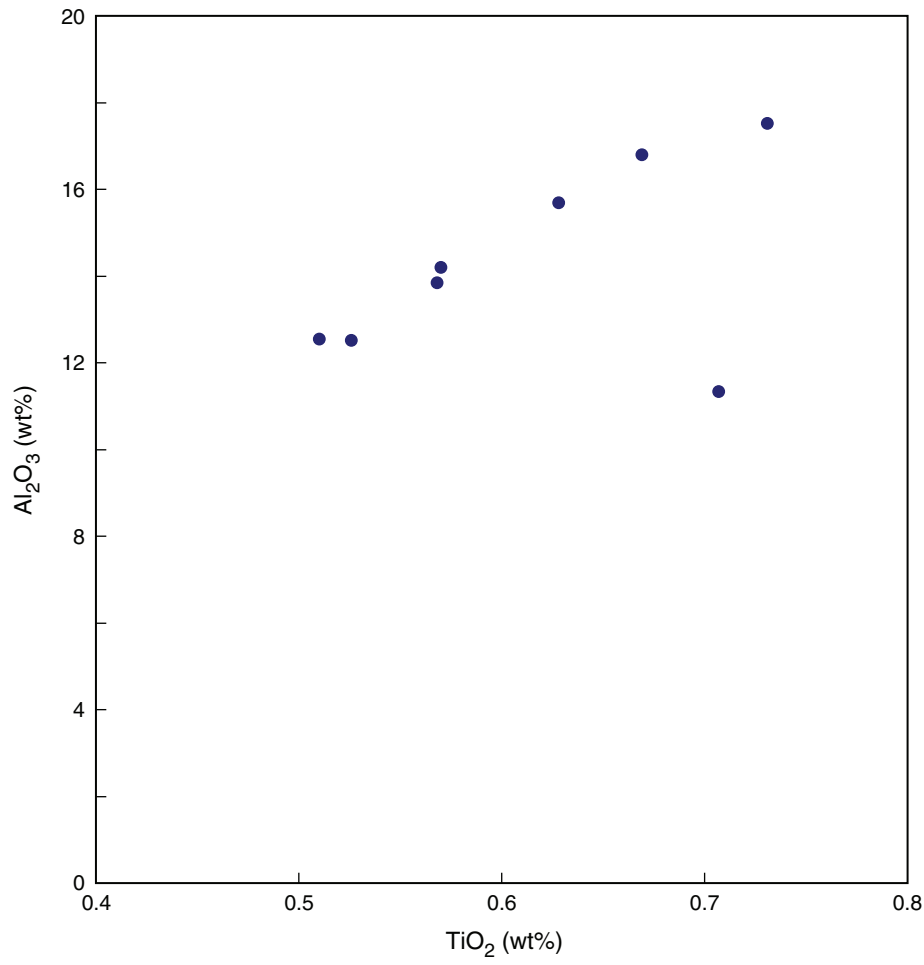
Figure F19. Plot of Al$_2$O$_3$ vs. depth. See Figure F3, p. 24, for the ages of units and the nature of interbedded coarser grained sediments.
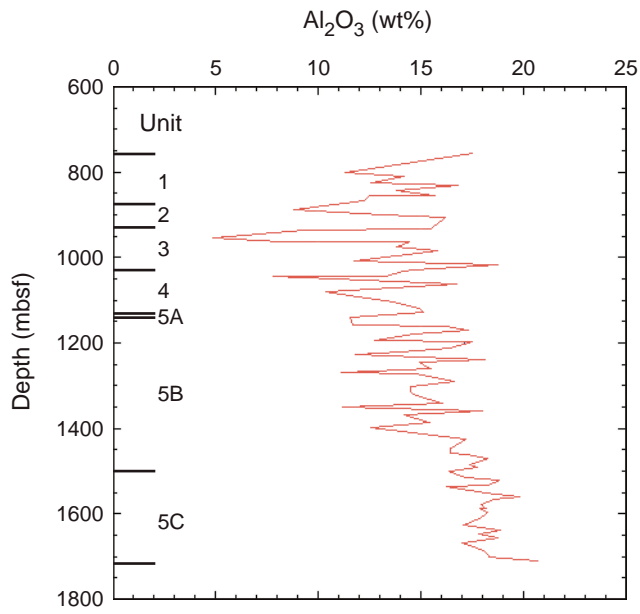
Figure F20. Plot of TiO$_2$ vs. depth. See Figure F3, p. 24, for the ages of units and the nature of interbedded coarser grained sediments.
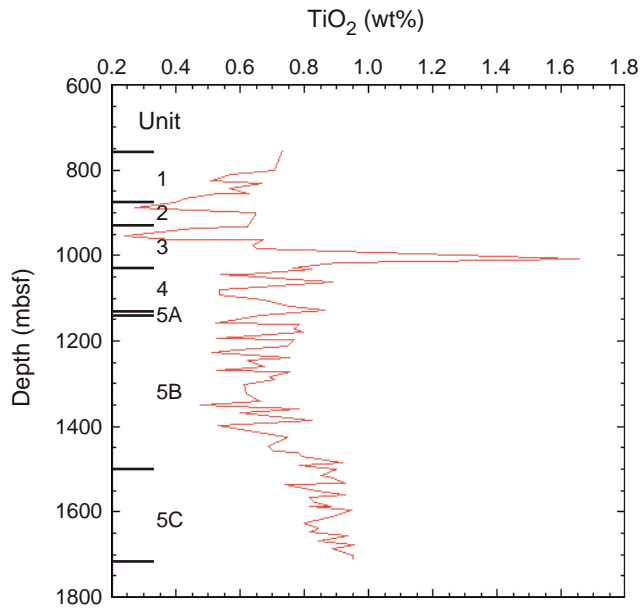
Figure F21. Plot of K$_2$O vs. depth. See Figure F3, p. 24, for the ages of units and the nature of interbedded coarser grained sediments.
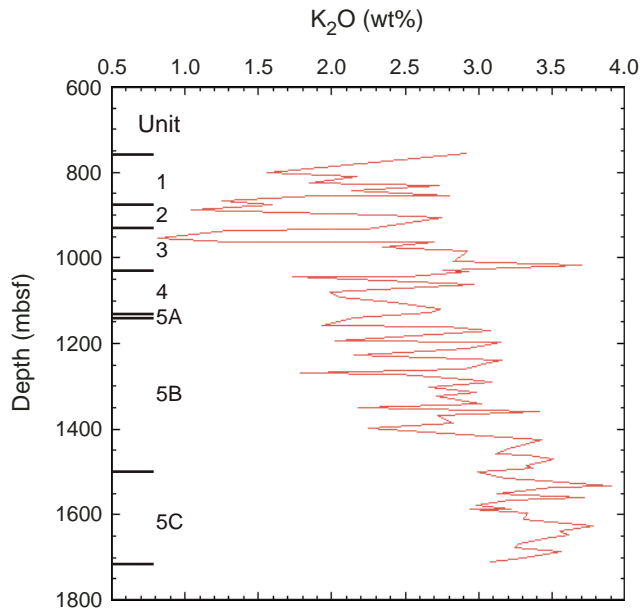
Figure F22. Plot of Fe$_2$O$_3$ vs. depth. See Figure F3, p. 24, for the ages of units and the nature of interbedded coarser grained sediments.
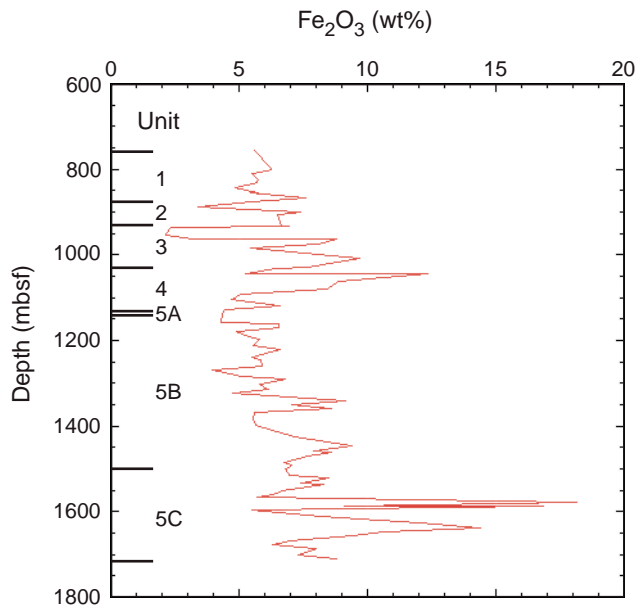
Figure F23. Plot of SiO$_2$ vs. depth. See Figure F3, p. 24, for the ages of units and the nature of interbedded coarser grained sediments.
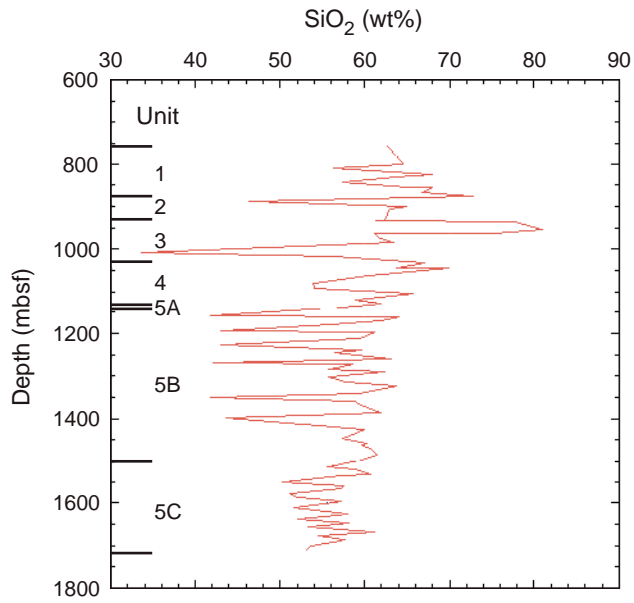
Figure F24. Plot of CaO vs. depth. See Figure F3, p. 24, for the ages of units and the nature of interbedded coarser grained sediments.
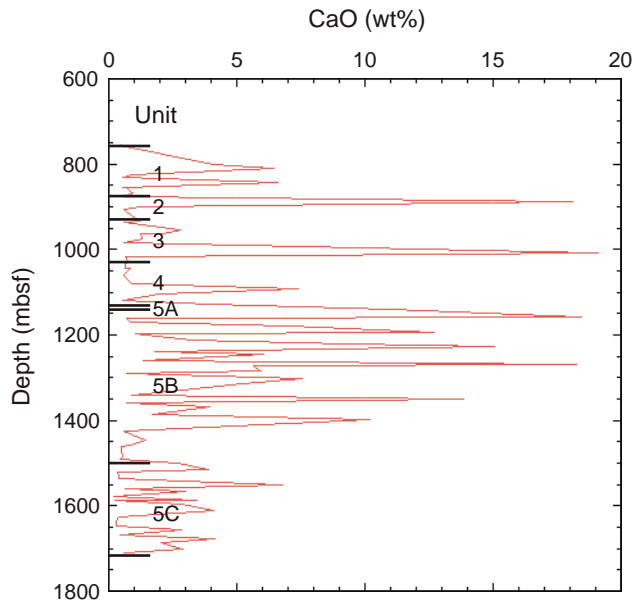
Figure F25. Plot of P_2O_5 vs. depth. See Figure F3, p. 24, for the ages of units and the nature of interbedded coarser grained sediments.
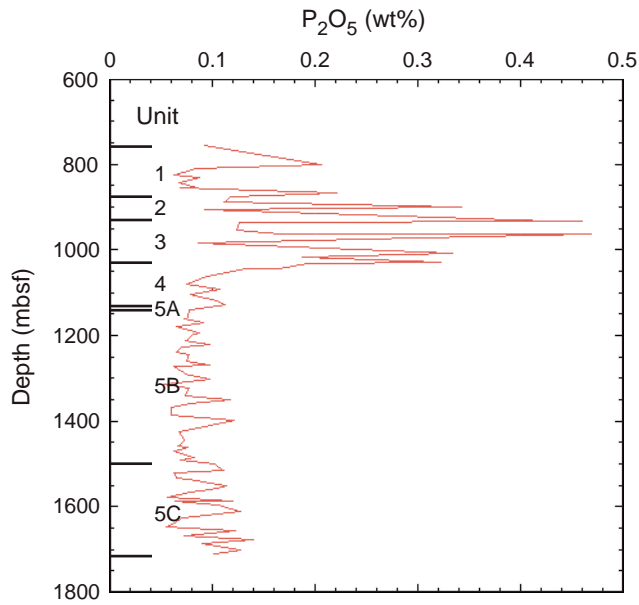
Figure F26. Plot of MnO vs. depth. See Figure F3, p. 24, for the ages of units and the nature of interbedded coarser grained sediments.
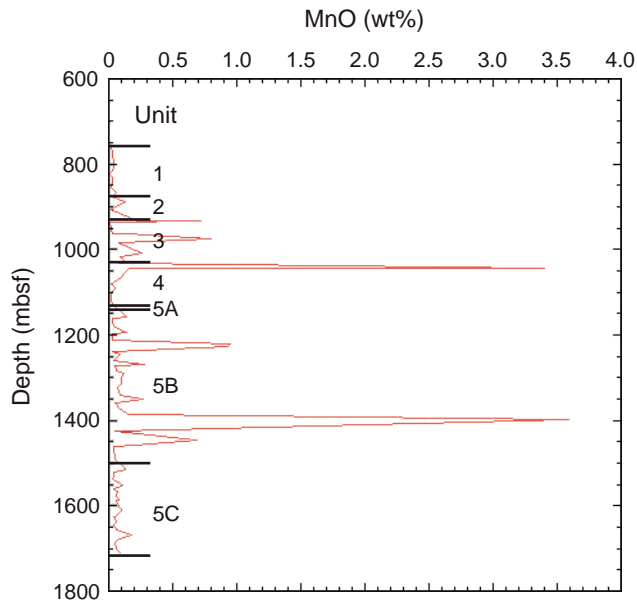
Figure F27. Plot of MgO vs. depth. See Figure F3, p. 24, for the ages of units and the nature of interbedded coarser grained sediments.
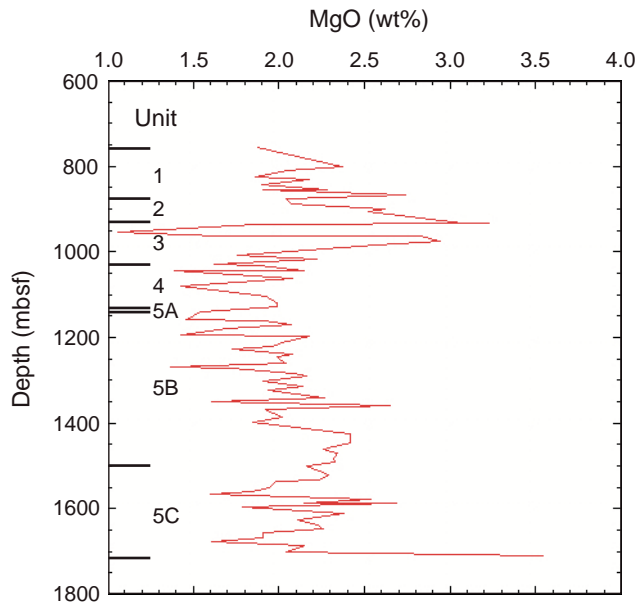
Figure F28. Plot of Na₂O vs. depth. See Figure F3, p. 24, for the ages of units and the nature of interbedded coarser grained sediments.
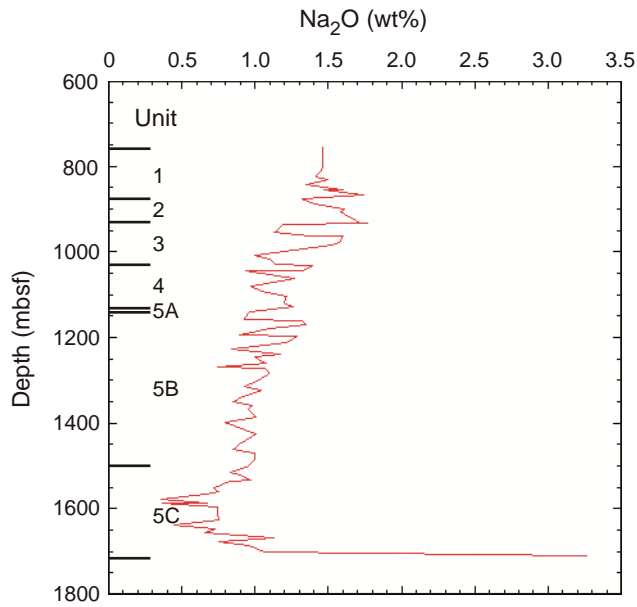
Figure F29. Plot of Rb vs. depth. See Figure F3, p. 24, for the ages of units and the nature of interbedded coarser grained sediments.
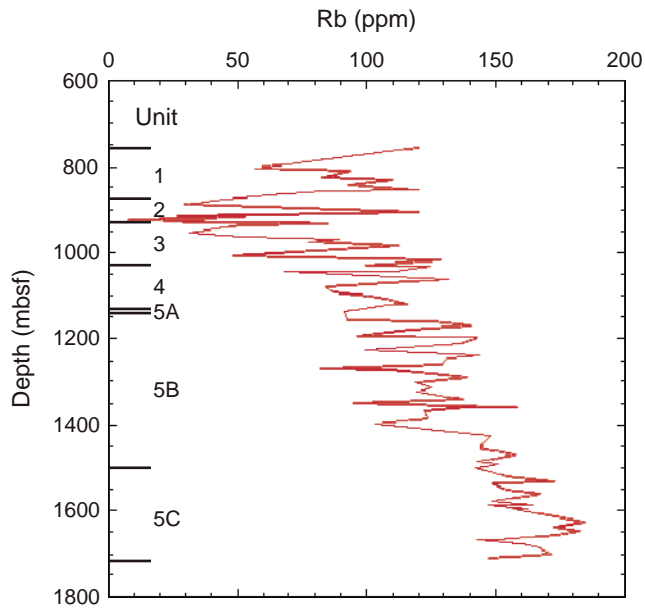
Figure F30. Plot of Cr vs. depth. See Figure F3, p. 24, for the ages of units and the nature of interbedded coarser grained sediments.
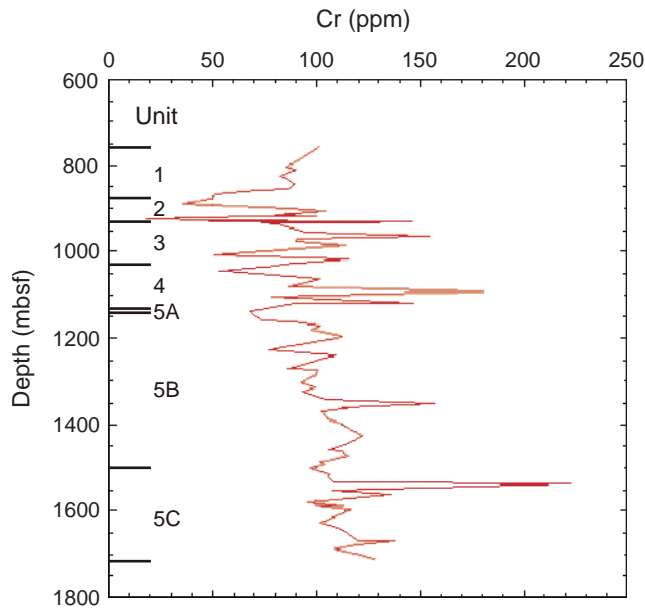
Figure F31. Plot of Ni vs. depth. See Figure F3, p. 24, for the ages of units and the nature of interbedded coarser grained sediments.
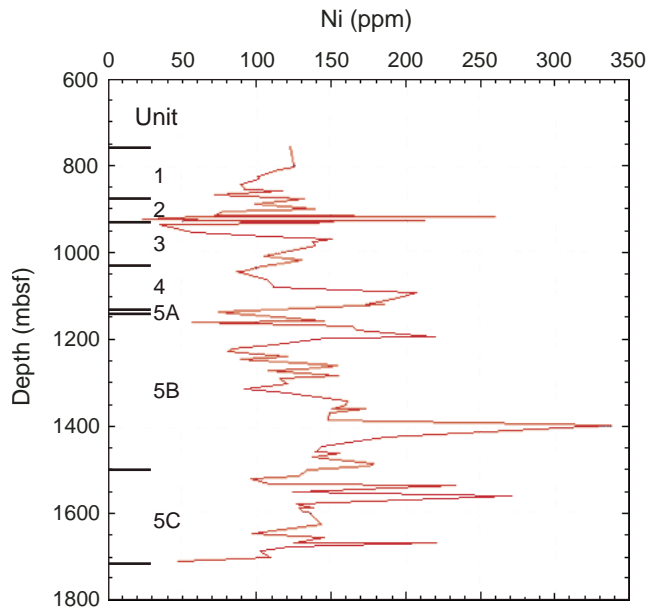
Figure F32. Plot of Zn vs. depth. See Figure F3, p. 24, for the ages of units and the nature of interbedded coarser grained sediments.
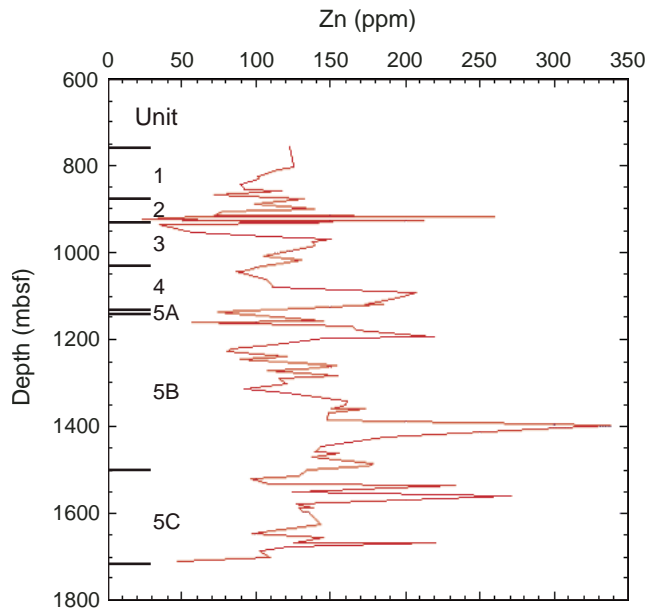
Figure F33. Plot of V vs. depth. See Figure F3, p. 24, for the ages of units and the nature of interbedded coarser grained sediments.
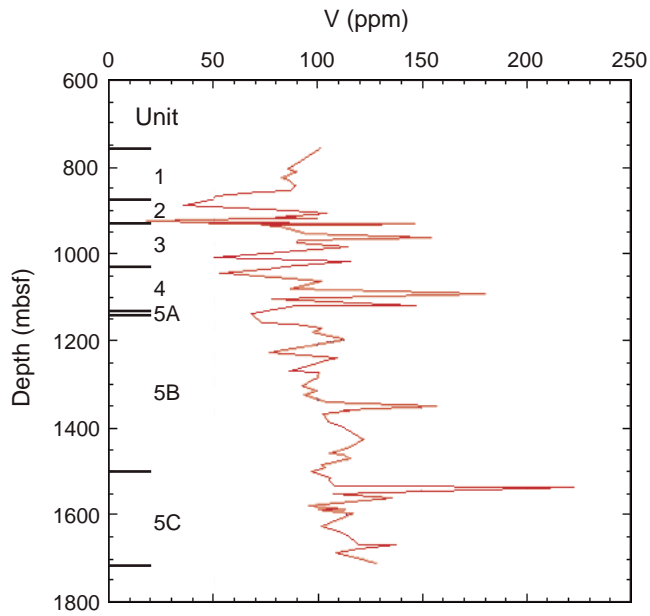
Figure F34. Plot of Ba vs. depth. See Figure F3, p. 24, for the ages of units and the nature of interbedded coarser grained sediments.
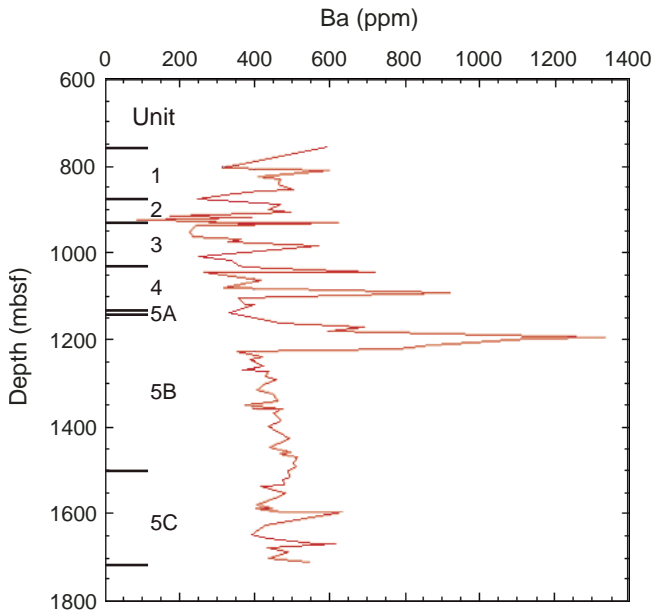
Figure F35. Plot of Zr vs. depth. See Figure F3, p. 24, for the ages of units and the nature of interbedded coarser grained sediments.
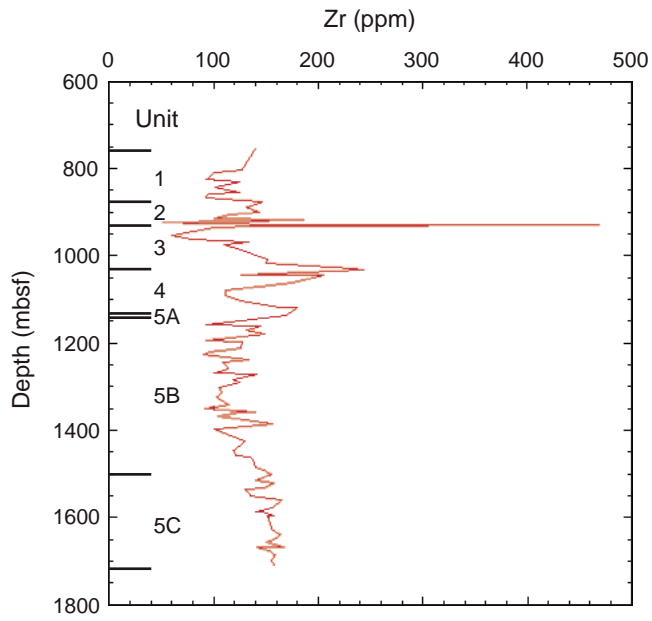
Figure F36. Plot of Cu vs. depth. See Figure F3, p. 24, for the ages of units and the nature of interbedded coarser grained sediments.
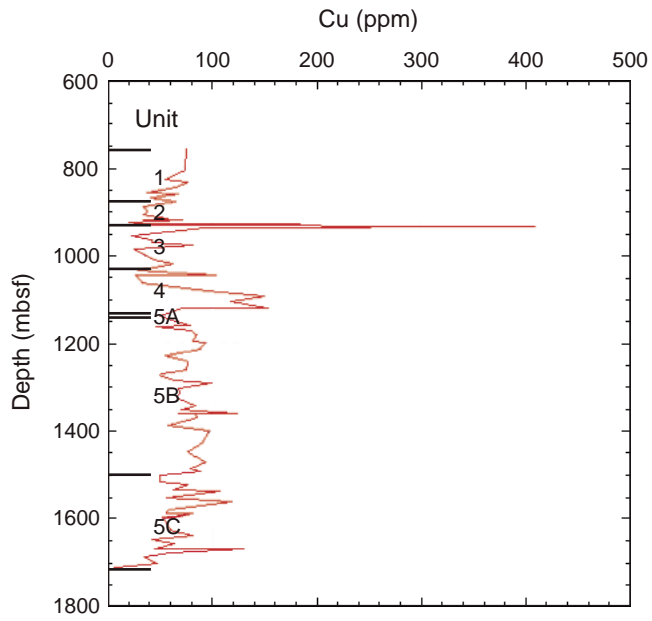
Figure F37. Plot of Ce vs. depth. See Figure F3, p. 24, for the ages of units and the nature of interbedded coarser grained sediments.
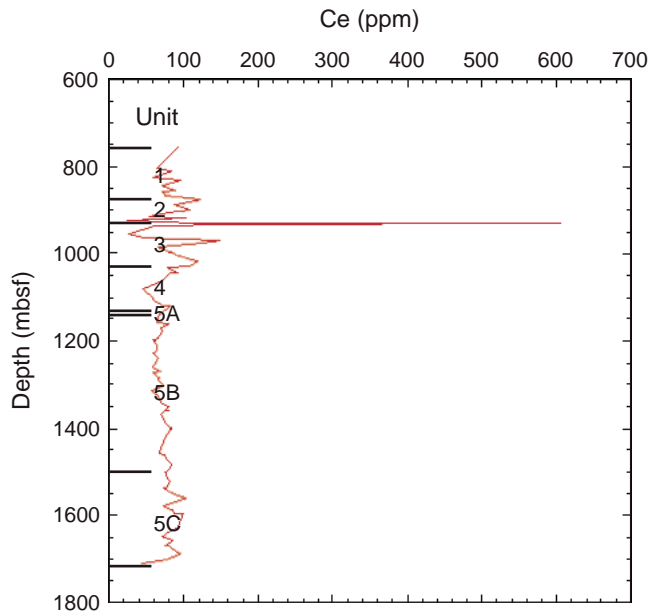
Figure F38. North American shale composite (NASC)-normalized plots for selected representative analyses from each lithologic Unit 1–5 at Site 1276. Normalizing values of the NASC are from Gromet et al. (1984). Normalizing values (in parts per million) are Sc = 14.90, Cr = 124.50, Zr = 200, Y = 21, La = 31.1, Ce = 66.7, Nd = 27.40, Sr = 142, Rb = 125, and Ba = 636.
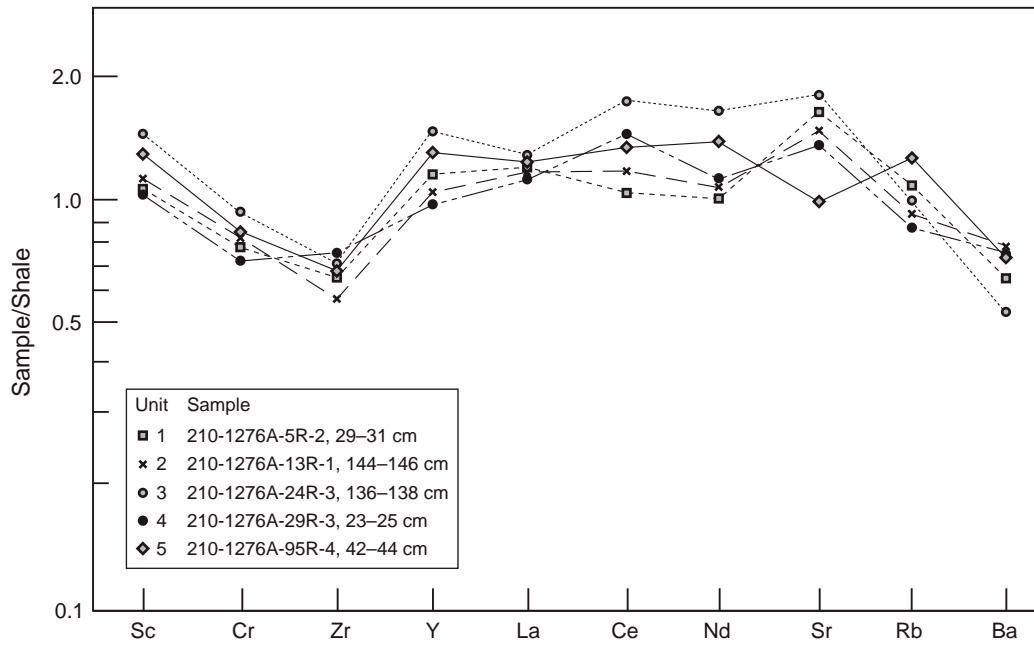
Table T1. Major and trace element analyses of fine-grained sediments, Site 1276. (See table note. Continued on next three pages.)

Core, section, interval (cm)	Sample number	Depth (mbsf)	Unit	Major element oxides (wt%)										Trace elements (ppm)		
				SiO$_2$	Al$_2$O$_3$	Fe$_2$O$_3$	MgO	CaO	Na$_2$O	K$_2$O	TiO$_2$	MnO	P$_2$O$_5$	Nb	Zr	Y
210-1276A-																
1W-2, 22–24	AR1	754.71		62.68	17.52	5.58	1.88	0.43	1.46	2.918	0.731	0.018	0.093	14.4	140.3	21.6
2R-1, 104–105	AR2	804.04		64.53	11.34	6.27	2.37	4.12	1.46	1.561	0.707	0.038	0.206	11.2	127.5	24.5
3R-2, 13–16	AR3	809.92		56.28	14.2	5.49	2.04	6.44	1.45	2.174	0.57	0.039	0.084	11.2	100.3	20.1
4R-4, 5–7	AR5	823.75	1	67.95	12.55	5.74	1.86	0.89	1.42	1.847	0.51	0.013	0.062	9.6	91.9	15.1
5R-2, 29–31	AR6	830.59		63.55	16.79	5.69	2.18	0.54	1.5	2.731	0.669	0.03	0.087	13.8	124.7	21.0
6R-3, 65–66	AR7	842.05		57.41	13.84	4.86	1.9	6.61	1.35	2.139	0.568	0.032	0.068	10.7	101.1	18.3
7R-6, 70–72	AR8	856.20		65.06	15.69	5.75	2.28	0.56	1.6	2.801	0.628	0.016	0.086	13.5	124.5	21.1
8R-2, 8–10	AR9	859.18		67.97	12.52	5.43	1.91	0.71	1.47	1.889	0.526	0.017	0.069	9.7	95.5	16.4
9R-1, 11–13	AR10	867.31		66.77	12.21	7.62	2.74	0.95	1.74	1.252	0.426	0.065	0.221	13.6	92.3	15.8
10R-1, 5–7	AR12	876.85		72.69	10.76	5.45	2.04	0.56	1.32	1.596	0.395	0.029	0.118	48.1	146.6	27.3
11R-1, 140–142	AR13	887.80		46.37	8.8	3.4	2.07	18.09	1.41	1.042	0.272	0.129	0.111	35.4	131.4	17.4
12R-4, 84–86	AR14	901.34		64.95	13.2	7.4	2.62	1.22	1.61	2.342	0.646	0.045	0.343	12.0	143.3	46.8
13R-1, 144–146	AR15	907.14		62.93	16.2	6.52	2.52	0.59	1.58	2.748	0.649	0.021	0.093	12.7	114.8	22.1
14R-1, 118–121	AR111	916.48		32.47	2.69	1.46	0.84	33.39	0.4	0.731	0.223	0.132	0.227	5.8	100.0	17.0
14R-2, 95–97	AR112	917.75		41.93	6.19	2.25	1.29	23.78	0.76	1.653	0.579	0.158	0.42	49.2	171.3	19.8
14R-2, 100–102	AR113	917.80	2	41.01	8.38	2.63	1.5	21.28	1.28	1.743	0.726	0.091	0.401	58.8	186.0	20.9
15R-1, 40–42	AR114	925.40		66.84	1.11	0.72	0.5	15.94	0.24	0.201	0.067	0.21	0.127	3.6	51.3	9.3
15R-1, 134–136	AR115	926.34		49.25	7.24	5.77	1.95	16.61	1.12	1.16	0.397	0.162	0.235	22.6	94.3	21.3
15R-1, 145–147	AR116	926.45		26.69	3.36	1.55	1.1	35.37	0.55	0.495	0.179	0.674	0.163	10.7	71.2	19.3
15R-2, 145–147	AR117	927.95		40.62	4.47	2.58	1.43	26.17	0.77	0.719	0.267	0.206	0.203	20.5	84.5	16.5
15R-3, 46–48	AR118	928.46		25.71	3.94	1.84	1.44	33.92	0.62	0.786	0.447	0.417	0.427	52.6	108.1	20.1
15R-3, 103–106	AR119	929.03		39.87	6.78	3.47	1.92	22.96	1.04	1.03	0.436	0.437	0.294	54.6	161.9	30.4
15R-3, 120–122	AR120	929.20		48.27	11.2	4.91	2.68	13.19	1.69	1.602	0.942	0.314	0.554	124.8	294.9	25.4
15R-4, 124–126	AR121	930.74		63.39	11.86	3.78	2.43	6.05	1.55	2.081	0.626	0.116	0.85	38.1	201.5	90.2
15R-4, 133–135.9	AR122	930.83		51.48	8.96	10.53	3.51	9.6	1.65	1.997	1.31	0.377	5.183	232.9	468.7	94.6
15R-5, 65–66	AR16	931.65		62.38	15.43	6.65	3.08	1.19	1.72	2.235	0.625	0.233	0.431	11.9	139.5	60.8
15R-5, 75–76	AR17	931.75		61.4	15.24	6.94	3.23	1.27	1.77	2.087	0.606	0.724	0.46	12.0	140.2	70.1
16R-2, 71–73	AR18	936.71		77.78	9.29	2.37	1.86	0.62	1.19	1.29	0.455	0.013	0.126	8.4	99.6	20.3
17R-7, 29–31	AR20	952.60		80.93	4.87	2.15	1.06	2.8	1.13	0.818	0.24	0.016	0.124	3.9	59.7	11.5
18R-7, 27–29	AR21	962.20	3	75.36	8.28	3.27	1.65	2.08	1.38	1.306	0.391	0.026	0.168	6.7	79.8	16.5
19R-5, 25–27	AR22	969.42		61.16	14.45	8.79	2.83	1.26	1.6	2.7	0.673	0.148	0.469	12.0	134.2	61.0
20R-2, 99–101	AR25	975.44		61.96	13.83	8.07	2.94	1.32	1.58	2.345	0.639	0.8	0.246	11.7	109.9	37.0
21R-1, 76–78	AR26	983.46		63.47	15.79	5.44	2.57	0.59	1.52	2.927	0.651	0.079	0.086	11.7	124.3	19.2
23R-4, 68–70	AR27	1006.62		33.58	11.78	9.68	1.76	19.1	1	2.826	1.656	0.262	0.334	40.7	151.1	26.7
24R-3, 136–138	AR28	1015.96		56.6	18.75	8.82	2.22	0.63	1.1	3.703	0.9	0.085	0.187	17.8	150.5	32.5
25R-7, 32–34	AR29	1030.02		65.16	14.62	7.65	1.62	0.74	1.14	2.754	0.765	0.126	0.323	13.9	233.5	47.3
26R-1, 50–52	AR30	1031.30		67.01	14.15	6.39	1.89	0.64	1.39	2.932	0.826	0.083	0.193	16.4	243.4	29.8
27R-2, 54–57	AR32	1042.51	4	63.75	13.27	5.27	2.15	0.66	1.32	2.511	0.621	3.404	0.164	13.3	126.3	32.8
27R-4, 19–21	AR33	1045.10		69.89	7.79	12.35	1.39	0.87	0.94	1.734	0.541	0.155	0.131	10.2	204.5	19.1
29R-3, 23–25	AR34	1062.76		60.43	16.78	8.84	2.08	0.59	1.27	2.965	0.887	0.106	0.094	17.0	175.0	25.9
31R-2, 70–72	AR35	1081.20		53.92	10.35	8.41	1.43	0.93	0.97	1.985	0.538	0.024	0.075	9.4	111.3	23.3
32R-3, 91–93	AR36	1092.51		54.01	11.94	5.04	1.68	7.4	1.05	2.06	0.537	0.05	0.108	14.9	111.7	23.7
33R-5, 14–16	AR38	1104.34	5A	65.77	13.7	4.71	1.93	1.97	1.22	2.429	0.674	0.021	0.079	12.5	126.2	23.6
35R-1, 58–60	AR39	1117.98		59.01	14.94	6.59	1.99	0.55	1.2	2.741	0.756	0.016	0.105	13.3	163.9	24.6
35R-2, 89–91	AR41	1119.70		61.95	15.13	4.43	1.99	3.93	1.26	2.664	0.864	0.034	0.112	15.6	180.3	32.0
37R-1, 7–10	AR43	1136.47		55.78	11.59	4.35	1.54	11.07	0.96	2.142	0.663	0.08	0.077	12.3	168.7	27.0
39R-3, 77–79	AR47	1159.00		41.79	11.69	4.3	1.46	18.43	0.93	1.935	0.524	0.14	0.076	9.0	92.3	25.2
39R-4, 102–104	AR48	1160.73		64.09	16.27	6.53	1.92	0.68	1.32	2.788	0.785	0.028	0.072	13.8	144.5	28.3
40R-4, 99–101	AR49	1170.35		61.91	17.34	6.55	2.07	0.92	1.35	3.081	0.77	0.026	0.091	14.0	131.4	27.5
41R-3, 42–44	AR50	1177.86		55.82	14.63	4.91	1.69	7.08	1.09	2.685	0.798	0.042	0.065	13.2	148.8	24.9
42R-7, 30–33	AR51	1193.03		42.98	12.76	5.56	1.43	12.71	0.89	2.022	0.527	0.14	0.088	9.2	92.1	25.0
43R-4, 47–49	AR53	1198.42		61.13	17.53	5.8	2.18	1.07	1.29	3.149	0.769	0.026	0.081	13.4	126.9	24.2
44R-5, 132–134	AR55	1210.60		59.37	16.35	5.55	2.01	3.26	1.21	2.917	0.743	0.033	0.074	13.2	126.2	24.4
45R-6, 64–66	AR56	1221.09		49.34	13.93	6.59	1.96	9.37	0.99	2.488	0.587	0.95	0.097	10.1	95.0	26.4
46R-3, 104–106	AR57	1226.49		43.08	11.82	6.18	1.73	15.05	0.84	2.156	0.514	0.927	0.07	8.5	89.7	24.4
47R-4, 120–122	AR58	1237.77	5B	59.68	18.11	5.5	2.08	1.81	1.17	3.161	0.754	0.029	0.065	13.3	134.2	24.0
48R-2, 97–99	AR59	1244.21		56.38	14.92	5.83	1.99	6.07	1	3.06	0.626	0.089	0.078	10.7	108.8	25.8
49R-6, 48–51	AR61	1259.38		63.19	15.52	5.88	2.04	1.37	1.08	2.895	0.675	0.039	0.075	13.3	113.8	21.6
50R-5, 60–62	AR62	1267.60		42.08	11.13	3.97	1.37	18.23	0.74	1.789	0.526	0.278	0.097	8.9	99.7	27.5
51R-2, 63–65	AR63	1272.83		58.68	14.79	4.23	1.73	5.65	1.07	2.452	0.757	0.046	0.062	12.2	140.9	23.5
52R-2, 61–63	AR64	1282.51		55.58	15.99	5.11	2.09	5.93	1.09	2.925	0.693	0.064	0.071	12.8	119.1	24.2
74R-3, 97–100	AR65	1291.06		62.33	16.65	6.8	2.16	0.71	1.07	3.088	0.71	0.121	0.074	14.7	125.5	25.2
54R-2, 55–57	AR66	1301.65		55.58	14.51	5.81	1.91	7.57	1.01	2.665	0.611	0.105	0.097	10.6	105.3	27.8
55R-3, 63–65	AR67	1312.83		57.87	14.48	6.17	2.14	5.22	0.93	2.986	0.617	0.097	0.052	10.4	107.3	20.0
56R-3, 85–87	AR68	1322.65		63.81	14.8	4.73	1.94	3.79	1.04	2.713	0.62	0.073	0.078	10.3	102.2	22.9
58R-3, 63–65	AR69	1341.73		59.35	16.09	9.16	2.27	0.88	0.89	3.021	0.664	0.095	0.074	12.1	114.4	27.3

Table T1 (continued).

Core, section, interval (cm)	Sample number	Depth (mbsf)	Unit	Trace elements (ppm)											
				Sr	Rb	La	Ce	Nd	Zb	Cu	Ni	Cr	V	Ba	Sc
210-1276A-															
1W-2, 22–24	AR1	754.71		161.0	119.9	38.8	92.3	32.8	122.8	74.7	46.2	101.1	227.4	591.9	16.8
2R-1, 104–105	AR2	804.04		267.2	56.9	29.5	64.1	31.8	125.2	73.9	102.3	85.8	126.3	315.0	15.2
3R-2, 13–16	AR3	809.92		517.4	94.2	35.2	84.3	30.4	114.8	67.2	47.8	89.9	220.2	599.7	15.3
4R-4, 5–7	AR5	823.75	1	182.4	83.2	25.0	60.3	21.6	100.8	55.3	49.1	82.4	148.2	409.7	12.3
5R-2, 29–31	AR6	830.59		191.5	109.8	36.9	96.2	32.2	101.3	76.2	58.9	86.1	147.3	468.3	15.6
6R-3, 65–66	AR7	842.05		479.5	93.2	31.6	71.9	28.2	89.6	65.4	38.0	89.1	209.2	466.6	15.9
7R-6, 70–72	AR8	856.20		198.9	119.8	37.8	88.7	32.9	91.8	37.3	45.5	86.6	168.1	504.4	14.9
8R-2, 8–10	AR9	859.18		181.5	82.8	25.9	72.4	23.4	117.6	67.3	42.1	71.5	157.6	410.8	12.7
9R-1, 11–13	AR10	867.31		180.7	61.6	30.6	74.4	29.6	71.7	41.0	112.0	51.1	93.1	317.5	11.6
10R-1, 5–7	AR12	876.85		235.3	44.8	47.3	123.0	49.0	132.4	64.5	94.7	48.9	66.6	249.4	15.3
11R-1, 140–142	AR13	887.80		470.2	29.6	47.1	87.3	30.8	99.2	34.3	64.9	35.5	59.9	468.3	6.3
12R-4, 84–86	AR14	901.34		251.2	89.9	55.4	108.8	56.7	139.0	37.8	85.3	86.9	117.0	436.5	18.6
13R-1, 144–146	AR15	907.14		192.6	119.8	38.1	78.9	33.6	76.9	33.3	84.6	104.5	347.8	496.1	16.9
14R-1, 118–121	AR111	916.48		383.0	26.4	27.8	54.5	29.0	71.9	57.7	49.1	79.8	70.3	174.5	7.5
14R-2, 95–97	AR112	917.75		387.9	47.9	41.7	94.3	39.0	259.6	33.5	90.9	100.3	116.2	392.0	8.5
14R-2, 100–102	AR113	917.80	2	377.0	53.1	45.3	103.1	44.9	61.0	70.8	517.1	69.1	137.9	373.7	9.5
15R-1, 40–42	AR114	925.40		218.0	7.9	15.8	24.6	14.4	24.0	20.0	16.5	18.0	17.4	87.8	1.7
15R-1, 134–136	AR115	926.34		422.4	37.2	38.8	84.7	38.1	99.2	30.6	92.2	50.9	167.8	296.1	10.8
15R-1, 145–147	AR116	926.45		505.4	21.1	36.3	64.3	30.8	54.5	39.6	47.1	36.4	69.3	193.3	9.9
15R-2, 145–147	AR117	927.95		486.0	24.3	32.3	64.7	30.0	50.7	48.6	56.3	45.0	153.1	240.5	6.5
15R-3, 46–48	AR118	928.46		607.7	22.9	45.9	88.9	43.4	212.9	184.1	63.1	86.2	238.5	264.7	8.8
15R-3, 103–106	AR119	929.03		454.6	34.5	48.7	99.5	45.9	89.2	41.4	87.1	48.0	118.9	295.3	10.1
15R-3, 120–122	AR120	929.20		545.6	40.8	70.2	147.4	58.9	128.6	72.6	139.1	48.7	598.2	472.5	6.4
15R-4, 124–126	AR121	930.74		329.2	72.1	145.5	271.9	153.1	121.4	68.6	79.3	94.4	329.8	374.1	20.4
15R-4, 133–135.9	AR122	930.83		669.7	71.6	277.3	605.6	258.6	149.4	47.8	92.9	146.0	242.9	623.4	21.7
15R-5, 65–66	AR16	931.65		305.2	84.8	59.0	125.9	63.4	134.0	361.5	107.2	115.1	103.3	358.1	24.6
15R-5, 75–76	AR17	931.75		335.4	81.1	71.1	160.2	73.9	140.2	408.5	89.5	73.2	121.9	549.5	23.3
16R-2, 71–73	AR18	936.71		200.6	50.9	25.1	61.4	24.5	35.4	92.1	30.3	81.7	84.1	245.5	10.7
17R-7, 29–31	AR20	952.60	3	188.4	31.3	15.4	26.1	12.7	58.1	22.2	18.6	95.1	53.9	227.2	5.7
18R-7, 27–29	AR21	962.20		208.4	51.9	20.2	46.8	19.1	107.9	42.5	37.0	154.5	107.3	233.0	10.2
19R-5, 25–27	AR22	969.42		308.5	89.5	65.8	147.9	66.9	150.7	41.9	83.2	90.4	135.3	362.6	17.4
20R-2, 99–101	AR25	975.44		305.9	77.6	46.3	125.5	45.0	137.5	81.5	95.3	89.8	128.7	327.3	16.0
21R-1, 76–78	AR26	983.46		251.9	112.4	31.7	67.3	29.5	139.3	24.4	43.8	114.6	297.5	569.1	17.4
23R-4, 68–70	AR27	1006.62		511.4	48.1	46.1	100.5	47.1	105.2	44.6	70.3	50.5	162.2	253.2	19.3
24R-3, 136–138	AR28	1015.96		227.5	129.1	42.7	118.9	43.9	130.7	62.9	81.9	115.4	140.5	339.5	23.0
25R-7, 32–34	AR29	1030.02		192.6	99.5	48.2	106.6	56.6	109.9	38.8	108.8	82.6	156.5	358.8	19.6
26R-1, 50–52	AR30	1031.30		215.2	124.6	33.9	78.4	34.3	103.1	29.1	62.8	81.1	121.7	373.7	18.0
27R-2, 54–57	AR32	1042.51	4	276.7	110.5	40.0	92.6	34.4	90.3	104.1	61.3	53.4	113.9	722.4	16.7
27R-4, 19–21	AR33	1045.10		152.2	68.3	22.0	82.7	22.6	86.8	26.5	69.9	56.5	213.3	266.8	12.8
29R-3, 23–25	AR34	1062.76		231.9	131.9	33.4	72.3	29.8	106.6	32.0	71.6	101.6	161.3	415.8	18.5
31R-2, 70–72	AR35	1081.20		171.6	84.0	24.1	45.7	22.9	111.4	96.7	273.8	87.0	305.0	317.3	11.3
32R-3, 91–93	AR36	1092.51		307.2	87.4	30.2	54.3	24.5	207.0	150.1	119.1	180.2	309.8	921.7	11.7
33R-5, 14–16	AR38	1104.34	5A	236.8	105.1	29.9	60.0	26.1	194.2	117.7	122.4	78.0	143.2	356.1	15.1
35R-1, 58–60	AR39	1117.98		215.1	115.9	28.8	73.8	27.8	173.4	154.3	120.8	147.1	228.6	376.2	18.2
35R-2, 89–91	AR41	1119.70		275.3	111.7	33.7	81.7	36.1	185.5	69.9	65.4	89.1	133.8	400.6	18.9
37R-1, 7–10	AR43	1136.47		334.4	91.3	31.8	68.1	34.2	74.3	50.3	67.2	68.1	96.5	330.8	16.0
39R-3, 77–79	AR47	1159.00		501.8	92.5	32.8	65.2	27.5	145.2	78.9	164.8	73.8	110.7	452.8	17.2
39R-4, 102–104	AR48	1160.73		244.8	126.0	39.3	80.0	33.7	57.0	46.3	64.2	89.0	136.3	470.0	18.0
40R-4, 99–101	AR49	1170.35		257.4	140.5	36.6	70.6	29.2	164.7	80.2	126.9	102.0	153.6	691.4	17.6
41R-3, 42–44	AR50	1177.86		318.8	116.7	32.7	71.3	30.5	166.7	85.6	215.4	97.4	146.0	594.9	18.0
42R-7, 30–33	AR51	1193.03		369.8	96.1	33.2	66.0	26.2	219.3	81.8	186.7	111.6	427.0	1332.9	15.1
43R-4, 47–49	AR53	1198.42		253.4	143.2	32.3	60.3	24.1	146.2	93.8	64.6	112.2	212.5	1129.7	17.9
44R-5, 132–134	AR55	1210.60		268.9	135.8	32.5	64.1	27.0	111.2	88.3	52.6	94.7	143.6	867.5	18.1
45R-6, 64–66	AR56	1221.09		354.4	114.8	32.3	65.4	29.9	82.9	67.5	79.5	83.7	134.5	780.7	17.2
46R-3, 104–106	AR57	1226.49		375.8	99.4	32.3	59.2	25.5	80.5	54.8	69.0	76.9	112.7	352.9	15.6
47R-4, 120–122	AR58	1237.77	5B	236.7	143.9	33.8	66.7	28.7	120.9	75.4	74.6	109.4	161.4	420.4	19.4
48R-2, 97–99	AR59	1244.21		267.2	131.3	33.3	65.0	30.6	88.9	76.7	77.3	104.0	155.3	389.7	17.1
49R-6, 48–51	AR61	1259.38		214.2	129.6	31.8	60.3	27.4	153.6	75.3	180.1	92.9	158.1	422.4	16.9
50R-5, 60–62	AR62	1267.60		416.6	82.6	36.3	70.5	33.2	130.6	51.1	97.8	86.5	171.9	367.4	15.8
51R-2, 63–65	AR63	1272.83		312.0	109.3	29.5	59.1	27.0	107.6	50.0	71.2	100.5	140.6	438.3	16.4
52R-2, 61–63	AR64	1282.51		266.3	130.7	34.3	68.2	30.8	155.2	64.1	100.6	99.7	171.3	432.2	18.0
74R-3, 97–100	AR65	1291.06		203.8	138.8	33.6	67.3	29.8	115.6	98.7	116.7	96.8	173.6	457.8	18.0
54R-2, 55–57	AR66	1301.65		280.5	119.2	36.5	72.7	34.9	121.1	66.9	122.3	92.2	142.3	424.5	16.0
55R-3, 63–65	AR67	1312.83		234.1	125.1	30.5	57.6	26.3	92.0	68.3	102.1	99.2	137.0	407.3	16.3
56R-3, 85–87	AR68	1322.65		227.3	119.4	33.7	65.1	29.7	121.0	66.6	96.6	93.1	148.4	449.0	16.9
58R-3, 63–65	AR69	1341.73		189.3	137.4	37.0	70.7	33.9	160.8	83.7	206.4	104.2	171.4	463.5	18.1

Table T1 (continued).

Core, section, interval (cm)	Sample number	Depth (mbsf)	Unit	Major element oxides (wt%)										Trace elements (ppm)		
				SiO_2	Al_2O_3	Fe_2O_3	MgO	CaO	Na_2O	K_2O	TiO_2	MnO	P_2O_5	Nb	Zr	Y
78R-5, 83–85	AR70	1348.96		41.88	11.18	7.03	1.61	13.83	0.85	2.176	0.476	0.272	0.118	7.8	91.7	33.8
60R-4, 102–104	AR71A	1359.12		59	17.97	8.6	2.65	0.7	0.98	3.417	0.783	0.052	0.078	14.7	139.8	28.1
60R-4, 102–104	AR71B	1359.12		48.35	16.42	7.73	1.59	5.18	0.66	3.1	0.816	0.07	0.13	15.9	136.3	29.6
60R-4, 102–104	AR71C	1359.12		58.05	16.38	6.53	2.44	2.7	1.08	3.306	0.722	0.075	0.083	12.2	125.2	27.1
61R-3, 32–34	AR72	1366.52		59.65	14.17	5.6	1.92	3.96	0.95	2.725	0.6	0.067	0.06	10.4	104.2	21.4
63R-3, 54–56	AR73	1386.04		61.98	15.44	5.57	2.02	1.71	1.01	2.83	0.825	0.158	0.06	14.1	156.3	26.9
64R-5, 105–107	AR74	1399.25		43.63	12.55	5.63	1.85	10.18	0.8	2.247	0.534	3.588	0.121	9.7	100.8	34.2
67R-4, 48–51	AR76	1425.88	5B	59.94	17.17	7.21	2.42	0.6	1.01	3.431	0.747	0.05	0.068	13.0	130.5	27.8
69R-4, 36–38	AR77	1444.66		57.39	16.42	9.4	2.42	1.43	0.9	3.199	0.687	0.688	0.072	11.8	118.4	26.4
70R-6, 25–27	AR78	1457.25		60.31	16.43	7.88	2.28	0.8	0.87	3.112	0.708	0.205	0.066	12.7	121.3	27.0
71R-3, 8–10	AR79	1462.28		59.65	17.24	8.58	2.26	0.49	0.85	3.348	0.781	0.043	0.076	15.1	135.5	26.7
72R-2, 89–91	AR80	1471.29		60.77	18.25	7.64	2.34	0.48	1	3.514	0.792	0.043	0.062	14.4	137.7	27.1
73R-4, 106–108	AR81	1484.06		61.57	17.4	6.77	2.32	0.54	1	3.324	0.919	0.045	0.082	16.5	139.7	29.1
74R-3, 97–100	AR82	1492.07		60.4	17.73	7.04	2.33	0.47	0.98	3.37	0.783	0.045	0.069	16.7	149.2	28.4
75R-2, 113–115	AR83	1500.33		59.28	16.39	6.79	2.16	2.74	0.95	2.996	0.9	0.095	0.102	19.6	154.4	29.6
76R-5, 131–133	AR84	1514.61		55.53	17.16	6.97	2.26	3.88	0.83	3.182	0.85	0.132	0.111	16.2	140.3	28.5
77R-4, 80–82	AR85	1522.20		59.03	18.83	8.5	2.29	0.35	0.9	3.451	0.893	0.037	0.063	16.5	157.1	25.6
78R-5, 83–85	AR86	1533.33		60.77	18.22	7.39	2.23	0.42	0.97	3.903	0.929	0.035	0.065	16.6	147.8	25.1
79R-1, 100–102	AR87	1537.20		57.04	16.28	8.32	1.98	0.4	0.82	3.497	0.742	0.025	0.077	13.0	130.0	21.3
80R-4, 35–38	AR89	1550.65		50.2	18.19	6.67	1.94	6.81	0.72	3.126	0.84	0.113	0.114	16.8	134.4	28.6
81R-4, 77–80	AR90	1560.57		57.62	19.82	6.31	1.84	0.63	0.75	3.724	0.928	0.041	0.098	17.2	164.5	30.0
82R-1, 11–13	AR91	1565.11		57.16	18.52	5.69	1.6	3.01	0.66	3.206	0.817	0.068	0.078			
83R-3, 73–75	AR92	1578.23		51.08	17.91	18.16	2.54	0.22	0.36	2.987	0.835	0.056	0.056	16.1	154.5	24.2
84R-2, 102–104	AR93	1586.72		52.01	18.2	9.08	2.15	3.43	0.67	3.219	0.883	0.076	0.12	17.3	140.6	30.4
85R-1, 62–64	AR94	1588.32		52.15	17.89	16.84	2.69	0.23	0.37	2.945	0.817	0.064	0.064	15.5	146.9	27.2
86R-2, 110–112	AR95	1597.40	5C	57.31	18.27	5.5	1.79	2.91	0.74	3.335	0.947	0.071	0.106	20.0	157.7	29.7
86R-2, 110–112	AR96	1597.40		51.55	17.84	8.19	2.38	4.1	0.74	3.313	0.886	0.096	0.128	18.1	150.8	29.9
89R-1, 120–122	AR97	1624.80		57.98	17.09	12.06	2.11	0.42	0.75	3.785	0.802	0.043	0.07	15.4	155.2	29.0
90R-4, 108–110	AR99	1638.85		52.1	18.85	14.42	2.23	0.29	0.45	3.55	0.843	0.062	0.062	16.4	164.3	26.1
91R-3, 100–102	AR100	1646.80		58.17	17.81	10.61	2.26	0.32	0.73	3.615	0.817	0.043	0.055	15.8	158.7	25.7
92R-2, 98–102	AR101	1654.98		53.22	18.76	9.41	1.91	2.87	0.66	3.443	0.935	0.064	0.123	18.7	150.5	30.3
93R-4, 72–75	AR102B	1667.32		61.68	16.43	6.82	1.65	0.93	1.02	2.963	0.752	0.037	0.117	14.2	141.5	35.9
93R-4, 72–75	AR103	1667.32		61.25	17	6.95	1.91	0.45	1.13	3.276	0.845	0.176	0.072	15.0	168.0	26.6
94R-4, 8–12	AR104	1676.23		54.5	17.6	6.31	1.61	4.15	0.75	3.251	0.956	0.081	0.14	19.8	154.3	32.6
95R-4, 42–44	AR106	1685.98		57.78	18.08	8.01	2.15	2.05	0.96	3.561	0.888	0.054	0.09	18.3	159.0	29.5
97R-1, 110–113	AR108	1701.60		53.51	18.29	7.29	2.04	2.91	1.07	3.3	0.952	0.062	0.127	19.5	154.9	29.9
98R-1, 56–59	AR109	1710.66		53.13	20.68	8.81	3.54	0.62	3.26	3.078	0.951	0.089	0.101	18.9	157.8	22.9

Note: Analyses by X-ray fluorescence at the School of GeoSciences, University of Edinburgh, United Kingdom.

Table T1 (continued).

Core, section, interval (cm)	Sample number	Depth (mbsf)	Unit/ subunit	Trace elements (ppm)											
				Sr	Rb	La	Ce	Nd	Zb	Cu	Ni	Cr	V	Ba	Sc
78R-5, 83–85	AR70	1348.96		326.4	94.8	41.2	79.8	35.4	160.4	70.1	224.0	157.0	466.5	375.9	15.8
60R-4, 102–104	AR71A	1359.12		183.6	152.3	40.1	76.4	34.8	150.1	123.9	163.2	112.8	176.5	474.7	19.5
60R-4, 102–104	AR71B	1359.12		163.5	157.8	37.2	80.3	37.3	151.4	67.9	192.6	113.4	214.9	393.9	19.4
60R-4, 102–104	AR71C	1359.12		209.6	139.0	39.6	75.3	35.7	172.9	84.3	160.8	117.4	166.6	468.7	19.7
61R-3, 32–34	AR72	1366.52		220.7	122.1	33.4	69.7	31.3	149.0	85.3	303.1	102.5	158.7	450.6	18.2
63R-3, 54–56	AR73	1386.04		194.8	123.3	35.4	75.4	32.3	147.7	57.0	89.4	104.9	153.6	468.4	17.5
64R-5, 105–107	AR74	1399.25		250.0	103.4	41.3	84.5	37.0	337.6	97.1	264.3	112.8	201.0	436.8	16.1
67R-4, 48–51	AR76	1425.88	5B	188.4	147.8	41.6	75.2	35.5	185.7	90.7	153.8	122.0	183.4	492.3	19.6
69R-4, 36–38	AR77	1444.66		184.8	144.7	35.6	70.5	32.9	143.1	76.4	187.9	113.7	150.9	439.4	18.8
70R-6, 25–27	AR78	1457.25		183.0	144.7	36.7	68.2	32.6	139.1	84.3	147.4	105.6	165.0	497.5	18.1
71R-3, 8–10	AR79	1462.28		154.0	150.2	37.9	74.6	34.4	156.1	86.9	116.1	112.5	162.8	469.8	20.3
72R-2, 89–91	AR80	1471.29		181.6	157.3	38.2	76.8	35.2	137.8	93.8	153.5	115.7	162.2	513.5	20.9
73R-4, 106–108	AR81	1484.06		184.9	143.2	41.1	84.0	38.7	178.5	79.2	137.5	101.6	182.2	503.3	19.8
74R-3, 97–100	AR82	1492.07		175.3	150.9	39.3	82.4	36.0	174.8	89.1	141.6	103.8	168.3	510.5	19.1
75R-2, 113–115	AR83	1500.33		183.5	142.6	34.7	75.2	32.7	134.1	49.6	80.3	96.9	150.6	489.6	19.4
76R-5, 131–133	AR84	1514.61		202.4	151.5	37.5	79.5	32.7	127.7	49.6	72.6	106.2	168.2	492.8	20.9
77R-4, 80–82	AR85	1522.20		151.4	154.3	37.2	81.5	34.8	96.3	76.1	66.6	105.5	166.1	477.3	22.3
78R-5, 83–85	AR86	1533.33		174.1	172.5	37.2	78.4	34.4	109.6	62.0	90.9	108.8	185.5	478.0	21.5
79R-1, 100–102	AR87	1537.20		140.7	148.7	36.0	73.9	30.8	234.0	107.3	217.0	222.7	243.2	417.7	19.4
80R-4, 35–38	AR89	1550.65		209.5	154.3	41.5	88.4	38.4	123.9	55.9	71.1	107.7	165.1	482.3	22.5
81R-4, 77–80	AR90	1560.57		128.6	167.6	46.6	102.4	42.8	271.2	119.3	145.3	135.7	224.8	462.3	24.1
82R-1, 11–13	AR91	1565.11													
83R-3, 73–75	AR92	1578.23		97.1	148.7	33.8	73.9	32.5	127.2	59.1	87.0	95.6	153.1	406.9	21.8
84R-2, 102–104	AR93	1586.72		156.1	164.3	41.5	84.1	37.9	138.4	56.7	88.5	113.0	168.8	446.5	22.2
85R-1, 62–64	AR94	1588.32		98.9	146.9	38.9	85.1	36.8	128.4	81.3	81.1	100.3	167.4	401.0	21.0
86R-2, 110–112	AR95	1597.40	5C	154.9	162.3	41.5	87.5	37.2	131.8	60.8	88.0	115.6	177.6	476.2	21.9
86R-2, 110–112	AR96	1597.40		138.6	157.0	48.2	99.2	44.9	134.7	52.3	78.3	117.0	172.1	634.5	21.3
89R-1, 120–122	AR97	1624.80		120.0	184.6	42.0	92.5	40.1	143.6	60.6	97.7	101.9	165.5	428.0	18.8
90R-4, 108–110	AR99	1638.85		113.2	172.6	39.5	78.1	32.6	116.0	81.4	68.9	110.4	169.5	405.1	22.5
91R-3, 100–102	AR100	1646.80		119.6	182.6	34.3	71.1	30.4	97.0	42.7	89.1	114.5	165.8	391.9	20.6
92R-2, 98–102	AR101	1654.98		143.8	173.6	41.5	85.7	38.0	144.9	64.3	111.1	116.7	174.2	437.1	22.6
93R-4, 72–75	AR102B	1667.32		129.9	143.2	38.3	80.3	37.7	220.7	130.2	112.1	137.6	193.0	617.1	19.6
93R-4, 72–75	AR103	1667.32		83.9	150.7	35.1	76.0	32.3	125.3	44.7	127.3	119.8	178.1	567.0	18.7
94R-4, 8–12	AR104	1676.23		152.1	159.8	39.9	88.0	39.1	121.5	59.2	82.6	119.5	177.5	433.1	22.5
95R-4, 42–44	AR106	1685.98		129.4	167.4	41.1	95.9	39.0	102.4	35.4	77.6	108.7	171.9	491.5	23.3
97R-1, 110–113	AR108	1701.60		138.0	171.4	36.8	77.7	34.0	109.0	47.9	85.3	121.2	179.1	438.9	22.5
98R-1, 56–59	AR109	1710.66		94.6	146.9	19.5	44.4	18.6	47.1	6.8	99.5	128.3	212.9	547.5	22.6